



Contents lists available at ScienceDirect

# Sustainable Chemistry and Pharmacy

journal homepage: [www.elsevier.com/locate/scp](http://www.elsevier.com/locate/scp)



## Modification mechanism, heavy metal coupling and ecological security risk assessment of phosphogypsum utilization in self-leveling mortar

Chao-qiang Wang<sup>a,\*</sup>, Ze-yuan Wang<sup>a</sup>, Jing-wen Wang<sup>b</sup>, Huan Zhang<sup>c</sup>, De-ming Huang<sup>a</sup>

<sup>a</sup> School of Materials Science and Engineering, Chongqing Jiaotong University, Chongqing, 400074, China

<sup>b</sup> School of Materials Science and Engineering, Tongji University, Shanghai, 200092, China

<sup>c</sup> Institute of Technical Information for Building Materials Industry of China, Beijing, 100024, China



### ARTICLE INFO

Handling Editor: Borhane Mahjoub

**Keywords:**

Phosphogypsum  
High efficiency modified  
Heavy metals risk assessment  
Self-leveling mortar

### ABSTRACT

Few researches on high efficiency modified phosphogypsum (MPG) and its resource utilization in building materials. This article investigated the effects of different lower temperatures and drying times on the thermodynamic modification mechanism of macroscopic performance and microscopic structure of MPG, and investigates its application in phosphogypsum-based self-leveling mortars (PBSLM). Then, the coupling mechanism of characteristic heavy metals in the modification process (original-modification-hydration) was discussed, and the safety evaluation was conducted on the content of heavy metal elements in the sample. Data from microscopic analysis showed that with the increase of temperature and drying time, the strength of MPG blocks and the decomposition rate of dihydrate gypsum crystal both increased, while the particle size decreased. The degree of crystal decomposition becomes more complete as the temperature rises if the holding time remains constant. As well as, the MPG at 180 °C/7 h, 195 °C/7 h/10 h met the Chinese standard of “*Calcined gypsum*” (GB/T9776). The heavy metal elements in MPG decreased obviously, caused by the substitution solid solution formed by Ca<sup>2+</sup> and Fe<sup>3+</sup> and heavy metal ions and the adsorption of calcium sulfate hemihydrate crystals. After hydration of MPG, As and Cd increased slightly because dicalcium phosphate was insoluble in water and soluble in acid, and iron oxide reduced and dissolved Cd. Then, the ecological hazards of heavy metals in hydrated MPG after hydration were evaluated. The results showed that there was no environmental safety problem in the hydrated MPG, but the As and Cr elements in it had an acceptable carcinogenic risk through oral intake. Based on ensuring the safety of MPG, MPG powder was used in PBSLM. The research demonstrates that the basic mechanical properties of the PBSLM produced, when the MPG powder content is 330 g, and cement is 40 g are the best. The heavy metal aqueous solution's leaching amount is lower than China's national standard limit value. (30min fluidity, 24 h-flexural and compressive strength were 154 mm, 5.7 MPa and 10.6 MPa). Finally, based on this research, a set of general evaluation system for safe utilization of solid waste was established according to national standards. This provides theoretical support for the research of heavy metal in PG at low temperature and the ways of harmless and resource utilization.

\* Corresponding author.

E-mail address: [wcq598676239@126.com](mailto:wcq598676239@126.com) (C.-q. Wang).

## 1. Introduction

Phosphogypsum (PG) is an industrial solid waste generated during the wet process of phosphoric acid production (Ding et al., 2022). China's rapid industrialization following reform and opening up has positioned it as a major global phosphoric acid producer. However, this growth has also resulted in escalating side effects (Wei and Deng, 2022). Illustrated in Figs. 1 and 2, resourceful utilization pathways for PG primarily focus on cement retarders, construction materials, etc., and the quantity of resource utilization is relatively limited (Wang et al., 2023). The primary constituent of PG is  $\text{CaSO}_4 \cdot m\text{H}_2\text{O}$  ( $m = 0, 0.5, 2$ ), accompanied by trace quantities of detrimental impurities including phosphorus, fluoride, organic compounds, and heavy metals (such as arsenic, cadmium, chromium, mercury) (Gijbels et al., 2020a). According to the Chinese standard "Storage and Landfill Pollution Control Standard for Non-Hazardous Industrial Solid Wastes" (GB18599). PG is classified as industrial solid waste. The heavy metals contained in PG are exposed to the environment naturally (Wu et al., 2022a), gradually accumulating in water, air, and soil through processes like rainfall leaching and various atmospheric factors. This phenomenon unavoidably results in bioaccumulation within the food chain through biomagnification, posing a threat to organisms (Zhou et al., 2022). Excessive accumulation of PG can lead to severe ecological damage (Meskini et al., 2023). Given the intricate composition of PG, pre-treatment is imperative before its utilization. The pretreatment technologies for PG mainly include physical methods (Rosales et al., 2020), chemical processes (Mashifana, 2019), and calcination (Wu et al., 2022b). Physical methods are ineffective in removing heavy metals and organic impurities from PG. Chemical processes may lead to secondary pollution and lack strong operability, hindering significant development. Currently, calcination is the most prevalent treatment technology. Singh and Garg (2000) asserted that optimal mechanical properties of PG were attained at a calcination temperature of 1000 °C. Liu et al. (2020) demonstrated the complete removal of soluble phosphates from PG during a 2-h calcination at 600 °C, showcasing improved mechanical performance with escalating temperature. While calcination proved effective, its energy-intensive nature raised concerns about resource wastage. Consequently, some scholars shifted focus to high-efficiency calcination. Bumanis et al. (2018) studied the mechanical strength of PG calcined within the 100–180 °C range, revealing that, influenced by lignosulfonate-based plasticizers, the 14-day compressive strength could achieve 29 MPa. Geraldo et al. (2020) examined PG calcination

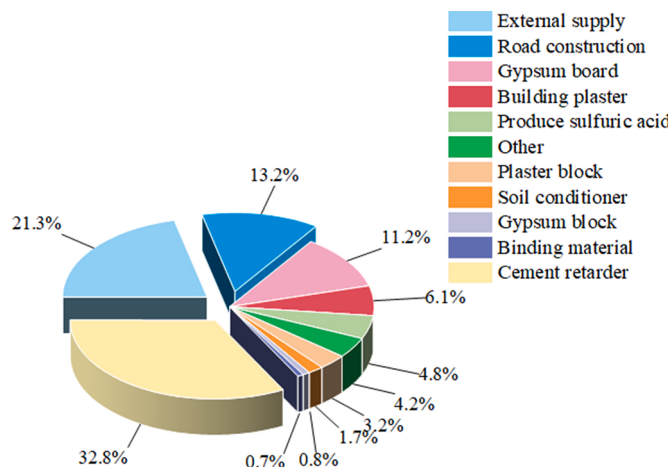


Fig. 1. Utilization ways and proportion of PG in China in 2020.

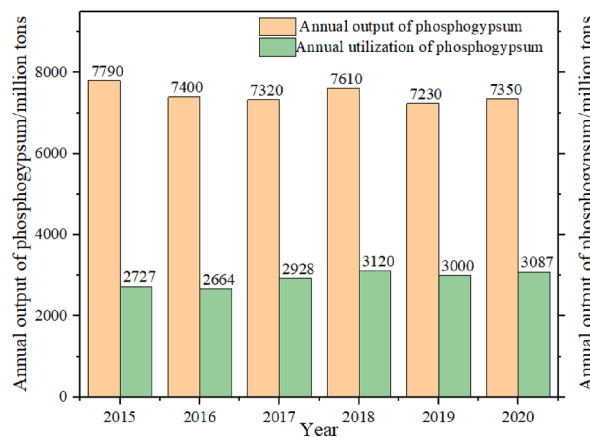


Fig. 2. PG of China output and resource utilization from 2015 to 2020.

at 120 °C, 150 °C, and 200 °C, noting a 28-day compressive strength of 6 MPa after 2 h at 150 °C. This fell short of the minimum 4 MPa compressive strength requirement stipulated in the Chinese standard for “Building Gypsum”.

Currently, there was relatively limited research on low-temperature (160°C–200 °C) calcination of PG, and the obtained PG powder exhibits suboptimal flexural and compressive strength. Importantly, the potential safety risks associated with heavy metals in PG subjected to low-temperature calcination had not garnered much attention from scholars (Degirmenci, 2008; Yang et al., 2009).

As shown in Fig. 2, the resourceful utilization of PG was primarily focused on areas such as construction, roads, agriculture, and the chemical industry. Self-leveling mortar was a self-leveling material with ultra-high fluidity and self-weight (Oliveira et al., 2022). It was a new type of building material and was widely used. The cement-based self-leveling mortar with Portland cement as the primary cementitious material was still widely used (Silva et al., 2023). Due to the high price of cement and other admixtures, and the poor wear resistance, there was a problem in its large-scale application (Saddam Alwan et al., 2022). Therefore, natural gypsum-based self-leveling mortar appeared. Gypsum-based self-leveling mortar came into being as cement-based self-leveling mortar (Zheng et al., 2021; Kalkan et al., 2022). However, with the introduction of the national ‘Dual-Carbon’ target, natural gypsum was limited. Therefore, people turned their research objectives to industrial dihydrate gypsums such as PG and desulfurization gypsum. Some scholars studied phosphogypsum-based self-leveling mortar (PBSLM) and confirmed that PG could be used as a substitute for natural gypsum (Wang and Jia, 2019; Yang et al., 2016). Zhang et al. (2021) showed that the compressive strength of gypsum-based self-leveling mortar was better when the content of PG was 55%. When a large amount of PG was used as raw material, the safety of heavy metals had not attracted people's attention.

To address the aforementioned research gaps, this study focuses on PG produced by a typical sulfur-containing chemical industry enterprise. It conducts an in-depth exploration into the impact of internal microstructural changes on the macroscopic properties of thermodynamic modification of PG under various modification conditions, including temperatures of 165 °C, 180 °C, and 195 °C, and calcination times of 5 h, 7 h, and 10 h. Additionally, the study emphasizes the coupling mechanism of heavy metals during the modification process. Furthermore, an assessment of the environmental hazards posed by heavy metals in modified phosphogypsum (MPG) is carried out. With a foundation of ensuring the environmental safety of MPG, the study applies MPG powder to gypsum-based self-leveling mortar, investigating the effects of different MPG contents and cement contents on the fundamental properties of PG-based self-leveling mortar (PBSLM), and comparing it economically with desulfurized gypsum-based self-leveling mortar. Finally, the study proposes a comprehensive model for evaluating the secure utilization of general solid waste, aligning with national standards. The results of this research contribute to bridging the existing knowledge gaps regarding the modification mechanisms and heavy metal coupling mechanisms during the High efficiency and low-cost modification of PG. This provides a theoretical basis for the widespread adoption of PG in various scenarios.

## 2. Materials and methods

### 2.1. Raw material

The PG selected for this research is from Fuling District, Chongqing, China. As shown in Fig. 3, the appearance is gray, showing a lumpy wet state. The results of the XRF test of PG in Table 1 show the content of SO<sub>3</sub>, CaO<sub>2</sub>, SiO<sub>2</sub>, F and P<sub>2</sub>O<sub>5</sub> in PG. Through XRD analysis, as illustrated in Fig. 4, the diffraction peaks in the PG are firm at 11.588°, 20.722°, 23.397°, 29.111°, and 31.104°. So, the main component of PG can be inferred to be CaSO<sub>4</sub>·2H<sub>2</sub>O and CaHPO<sub>4</sub>·2H<sub>2</sub>O (Li et al., 2022a,b,c).



Fig. 3. PG sample.

**Table 1**  
XRF test results of PG/%,mass.

Sample	SO <sub>3</sub>	CaO	SiO <sub>2</sub>	F	P <sub>2</sub> O <sub>5</sub>	K <sub>2</sub> O	Al <sub>2</sub> O <sub>3</sub>	Fe <sub>2</sub> O <sub>3</sub>	Others
PG	50.80	44.13	2.33	0.24	0.90	0.09	0.37	0.48	0.66

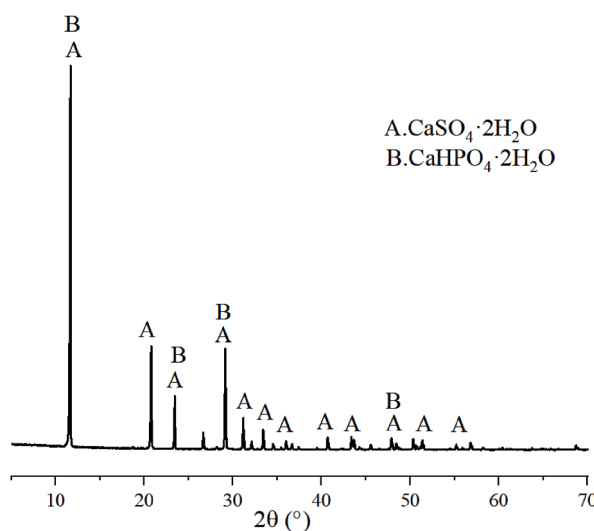


Fig. 4. XRD test results of PG.

## 2.2. TG analysis of PG

PG in the modified process due to temperature changes will produce semi-hydrated gypsum or anhydrous gypsum. From Fig. 5, the mass decreases of PG with the temperature increase from 120 °C. The weight loss rate of PG starts to accelerate when the temperature reaches 140 °C. From the DSC curve, when the temperature rises to 180 °C, the first endothermic peak appears in the PG sample. The dihydrate gypsum begins to dehydrate into a large amount of hemihydrate gypsum. The second endothermic peak appears when the temperature rises to 195 °C and above. This is because the hemihydrate gypsum in PG absorbs heat and dehydrates into anhydrous gypsum. When the temperature exceeds 200 °C, the weight loss curve of PG tends to be gentle, and the weight loss rate is 17.5%. The calcination temperature range of PG can be obtained from 140 °C to 195 °C.

## 2.3. MPG preparation process

The original PG was divided into three groups, with each group receiving 3 kg. Subsequently, the PG was placed in an oven and subjected to drying at temperatures of 165 °C, 180 °C, and 195 °C for durations of 5 h, 7 h, and 10 h, respectively. Following the drying process, the PG underwent modification and was introduced into an electromagnetic pulverizer for a grinding period of 3 min. After grinding, the processed samples were sifted using a round-hole sieve with a mesh size of 0.075 mm (in accordance with the specifi-

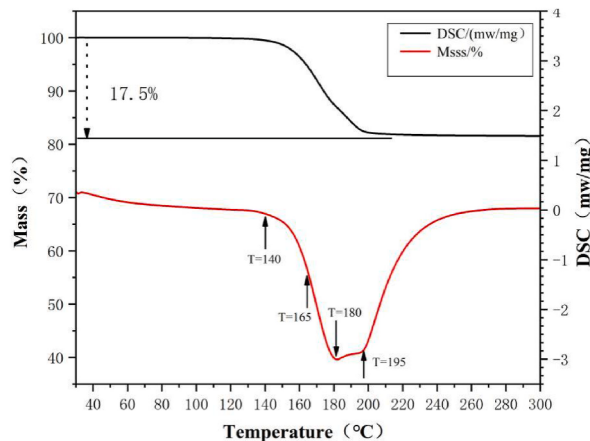


Fig. 5. TG analysis of PG.

cations outlined in GB/T9776). It was required that the surplus building gypsum powder passing through a square hole sieve with a mesh size of 0.2 mm should not exceed 10%. Ultimately, this procedure yielded a modified PG sample in a powdery form. Fig. 6 illustrate the step-by-step preparation process of MPG.

#### 2.4. Preparation of PG based self-leveling mortar (PBSLM)

##### 2.4.1. Raw material

The MPG powder with the best mechanical properties selected in this article is chosen as the main ingredients for the PPBSLM. The cement selected (P O 42.5) is produced by a cement factory in Chongqing. The heavy calcium powder is sourced from a manufacturer in Dandong City and is mainly used as a filling material. The fine aggregate used is sand with a particle size of 0–0.6 mm, sourced locally from Chongqing City.

##### 2.4.2. Additive

The water reducer is produced by Guangdong Longhu Technology Co., Ltd., and the P49 type water reducer is selected; the retarder is produced by Shenhui Gypsum Retarder Co., Ltd., and the SG retarder is selected; the cellulose ether is produced by Hercules Tianpu Chemical Co., Ltd., and the methyl hydroxypropyl cellulose ether with a viscosity of 400 MPa s (HPMC400) is selected; the defoamer is produced by Suzhou Xingbang Chemical Building Materials Co., Ltd., and the A-406 type is selected; the air-entraining agent is produced by Henan Wanshan New Material Technology Co., Ltd., and the sodium rosin air-entraining agent is selected.

##### 2.4.3. The preparation process of PBSLM

The formulation and mixing ratio of the PBSLM were shown in Table 2. Firstly, the experimental samples were prepared by uniformly mixing the selected MPG powder, ordinary Portland cement, sand (0–0.6 mm), and additives according to the prescribed ratio. Water was then added based on the water-cement ratio for testing and mixing to obtain the final product. Secondly, the physical properties of the PBSLM were mainly influenced by the dosage of MPG powder and cement. Finally, the formula of the PBSLM that met the specification requirements was determined. In each sample, the content of defoamer, water reducer, retarder, cellulose ether, and air-entraining agent was fixed at 0.5 g, 1.6 g, 0.3 g, 0.3 g, and 0.2 g, respectively. The preparation process of PBSLM was depicted in Fig. 7.

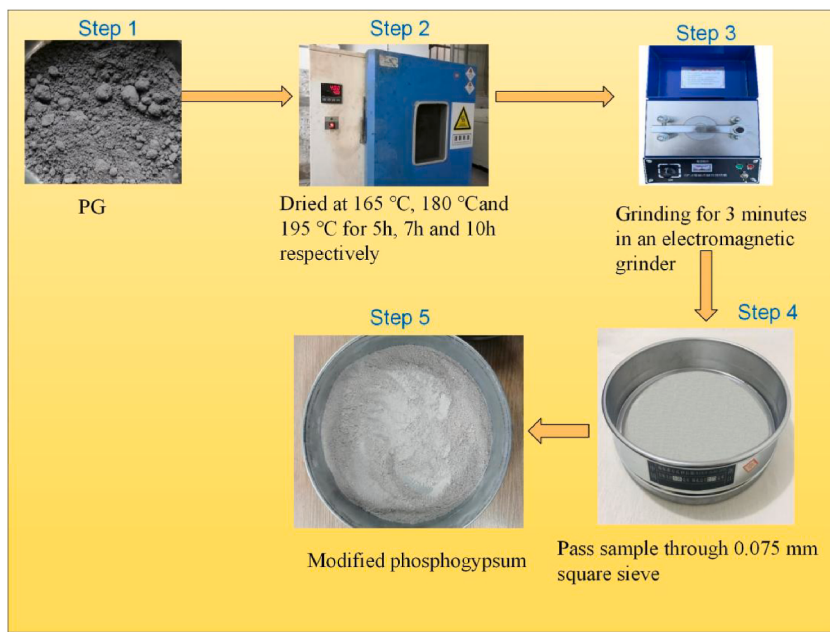


Fig. 6. Preparation process of MPG.

Table 2

The PBSLM mix proportion (g).

NO.	MPG	Cement	Heavy calcium powder	Sand	Additive	Water-binder ratio
PBSLM1	270	70	75	75	2.9	26%
PBSLM2	300	70	75	75	2.9	26%
PBSLM3	330	70	75	75	2.9	26%
PBSLM4	330	60	75	75	2.9	26%
PBSLM5	330	50	75	75	2.9	26%
PBSLM6	330	40	75	75	2.9	26%



Fig. 7. The preparation process of PBSLM.

## 2.5. Test method

### 2.5.1. Macroscopic tests

The dimensions of the specimens are 40 × 40\*160 mm, and parallel testing is conducted for each set, with a relative error controlled within 5%. The determination of standard consistency water content, setting time, flexural and compressive strength, and softening coefficient are all tested in accordance with the Chinese standard “Gypsum plasters—Determination of mechanical properties” (GB/T 17669.3). According to the Chinese standard “Gypsum-based self-leveling mortar” (JC/T1023) stipulated in China, the mechanical properties were tested. The main physical properties tested were 0min/30min fluidity, 24 h flexural and compressive strength.

### 2.5.2. Microscopic tests

**2.5.2.1. XRF.** The elemental composition analysis of PG is conducted using the X-ray Fluorescence Spectrometer produced (ARL Perform'X) by Thermo. The instrument's elemental analysis range covers Be–U, with a concentration range from ppm to 100%.

**2.5.2.2. XRD.** The phase composition of the samples is determined using the DMAX1400 X-ray diffractometer produced by Bruker AXS GmbH in Germany. The testing conditions involve a Cu target, continuous scanning, a scan speed of 10°/min, 2θ ranging from 5 to 90°, and a step size of 0.017°.

**2.5.2.3. FTIR.** The Nicolet iS50 Fourier Transform Infrared Spectrometer produced by Thermo Fisher Scientific is employed. The instrument specifications include a resolution of 0.09 cm<sup>-1</sup>, wavenumber accuracy of 0.005 cm<sup>-1</sup>, linearity less than 0.07% (according to ASTM1421 method), peak-to-peak noise ratio exceeding 55,000:1 (1-min scan, 4 cm<sup>-1</sup> resolution), spectral range of 7800–350 cm<sup>-1</sup> for the main unit, and diamond ATR range of 5000–80 cm<sup>-1</sup>.

**2.5.2.4. SEM/EDS.** Observation is performed using the VEGA 3 LMH scanning electron microscope produced by TESCAN in the Czech Republic. The instrument utilizes a tungsten filament electron gun, with a maximum acceleration voltage of 30 kV, point resolution of 3.0 nm @ 30 kV, and a diameter of 260 mm. Elemental analysis is conducted in conjunction with an energy-dispersive spectrometer.

**2.5.2.5. Gypsum phase composition analysis.** The SZ-GY2000SG gypsum phase composition analyzer produced by Shenzhen Guanya Technology Co., Ltd is used for testing. The instrument's gypsum triphasic detection range is 0.00001%–100%, with a heating source of molecular source and a temperature error of  $\leq 0.4$  °C.

### 2.5.3. Test methods for heavy metals

The determination of heavy metals in PG involves using an Agilent Inductively Coupled Plasma Optical Emission Spectrometer (ICP-OES) produced by Thermo Fisher Scientific. The testing is conducted following the Chinese protocol "Solid Waste Extraction Toxicity Leaching Method with Sulfuric Acid-Nitric Acid" (HJ/T299). The heavy metal leaching test of PBSLM in aqueous solution is carried out based on the Chinese standard "Solid Waste Extraction Toxicity Leaching Method - Horizontal Vibration Method" (HJ 577).

### 2.5.4. QA/QC procedure for the test process

To ensure the quality and reliability of the tests, procedural blanks, duplicates, and recovery tests are conducted. The deviation for duplicate tests is less than 5%. The spike recovery rates for Cr, As, Cd, and Hg range from 83.2% to 102.1%, with detection limits for all metals set at 0.01 mg/kg.

### 2.5.5. Ecological hazard assessment

PG contains some heavy metal elements, among which heavy metals with strong migration and transformation ability will be transferred to nature due to the random stacking and disposal of PG. In addition, PG will also enter the environment through rainwater, leaching, fertilization, etc. (Jalali et al., 2020). Complex migration and transformation in the food chain will eventually be transferred to the human body (Xu et al., 2018). Therefore, this research uses three environmental safety assessment models and the human health risk assessment model (USEPA) to analyze the safety problems of characteristic heavy metals in PG and MPG.

**2.5.5.1. Single factor index method.** The method is a common method for evaluating industrial solid waste pollution (Jia et al., 2022). It is as follows:

$$P_i = \frac{C_i}{S_i} \quad (1)$$

The meaning of  $P_i$  in the formula comes from the reference (Yang et al., 2022). Table 3 is the evaluation standard of  $S_i$  pollutant  $i$ , which values of this paper come from the Chinese standard ' Environmental quality standards for soils ' (GB15618).

**2.5.5.2. Potential ecological risk index.** This method calculates the risk index (RI) of different heavy metal elements through the background value of soil heavy metal elements and the content of heavy metal elements in samples (Chai et al., 2021). As the most commonly used assessment method of heavy metal pollution hazard, it has the principles of element richness and toxicity response (Wang et al., 2022).

$$C_f^i = \frac{C_s^i}{C_n^i} \quad (2)$$

$$E_r^i = T_r^i \times C_f^i \quad (3)$$

$$RI = \sum_1^n E_r^i \quad (4)$$

The meaning in the formula come from references (Dong et al., 2019). The standardized heavy metal toxicity coefficients are shown in Table 4.

**2.5.5.3. Geological accumulation index method.** The method refers to the determination of the degree of heavy metal pollution according to a particular relationship between the content of various heavy metals and their corresponding chemical background values, which can intuitively reflect the enrichment degree of heavy metals in sediments (Okoye et al., 2022; Liu et al., 2015). The formula is as follows.

**Table 3**  
Evaluation criteria for contaminants.

NO.	Cr	As	Cd	Hg
$S_i$	150.00	30.00	0.30	0.50

**Table 4**

Standardized heavy metal toxicity coefficient.

NO.	As	Cd	Cr	Hg
Toxicity coefficient	10	30	2	40

$$I_{geo} = \log_2 [C_i / (K \times B_i)] \quad (5)$$

The meaning and reference value of  $C_i$  in the formula come from references (Lü et al., 2021).

**2.5.5.4. Human health risk assessment.** The risk assessment of human health mainly evaluates the degree of heavy metal pollution by calculating the carcinogenic and non-carcinogenic risk index of human body from three aspects: oral intake, skin and inhalation exposure. The calculation process and formula are as follows.

$$ADD_1 = \frac{C \times IR \times EF \times ED \times CF}{BW \times AT} \quad (6)$$

$$ADD_2 = \frac{C \times ABS \times AF \times SA \times EF \times ED \times CF}{BW \times AT} \quad (7)$$

$$ADD_3 = \frac{C \times IR_1 \times EF \times ED}{BW \times AT \times PEF} \quad (8)$$

$$HQ_i = \frac{ADD_i}{RFD_i} \quad (9)$$

$$HI = \sum_1^n HQ_i \quad (10)$$

$$TCR = \sum ADD_i \times SF_i \quad (11)$$

The equivalence and significance of  $ADD_1$ ,  $ADD_2$ ,  $ADD_3$ ,  $HQ_i$ ,  $HI$ ,  $TCR$  in the formula come from references (Li and Ji, 2017; Mallongi et al., 2022; Wang et al., 2020). The values and sources of each parameter are exhibited in Tables 5–6.

**Table 5**

Parameter values and sources.

Item	Unit	Reference values	
		Grown-up	Kid
IR <sub>ing</sub>	mg·d	30	60
IR <sub>inh</sub>	m <sup>3</sup> ·d <sup>-1</sup>	7.63	20
EF	d·a	180	180
ED	years	24	6
AF	mg/cm <sup>2</sup>	0.07	0.2
BW	kg	70	15
AT	d	non-carcinogenic carcinogenic	8760 25,500
PEF	m <sup>3</sup> ·kg <sup>-1</sup>	1.36 E+0.9	1.36 E+0.9
SA	cm <sup>2</sup> ·d <sup>-1</sup>	5700	2800
ABS	—	0.001	0.001

**Table 6**

RFD and SF value of heavy metals.

	RFD <sub>1</sub>	RFD <sub>2</sub>	RFD <sub>3</sub>	SF <sub>1</sub>	SF <sub>2</sub>	SF <sub>3</sub>
Hg	3.00E-04	8.64E-04	3.00E-4	—	—	—
Cd	1.00E-06	1.00E-05	1.00E-03	6.30 E+00	3.80E-01	6.10 E+00
Cr	6.00E-05	2.86E-03	3.00E-04	4.20 E+01	2.00 E+00	5.00E-01
As	1.23E-04	3.00E-04	3.00E-04	1.50 E+01	3.66 E+00	1.51 E+00

### 3. Results and discussion

#### 3.1. Macroscopic properties of high efficiency modified PG

Gypsum's mechanical properties are related to the proportions of its three phases: hemihydrate gypsum, soluble anhydrite, and dihydrate gypsum (Li et al., 2022a,b,c). The calcination temperature and drying time are closely related to the composition of gypsum phases (Cao et al., 2022). Therefore, it is crucial to investigate the effects of different temperatures and drying times on the mechanical properties of PG. The basic mechanical properties of 9 groups ( $165^{\circ}\text{C}$  5 h/7 h/10 h,  $180^{\circ}\text{C}$  5 h/7 h/10 h,  $195^{\circ}\text{C}$  5 h/7 h/10 h) MPG samples are studied, as illustrated in Table 7.

##### 3.1.1. Standard consistency water consumption and setting time

From Table 7, temperature and holding time have a positive correlation with the water requirement of MPG. The setting time did not show a regular change. This is probably because the low drying temperature makes the MPG insufficiently calcined, so only a small amount of dihydrate gypsum dehydrates into hemihydrate gypsum, or it is related to the content and setting time of hemihydrate gypsum (Li et al., 2020). The detailed analysis can be found in 3.2 effect of macroscopic properties on microstructure.

##### 3.1.2. Flexural and compressive strength

As exhibited in Fig. 8 and Fig. 9, the flexural strength and compressive strength of the MPG specimens show a positive correlation with the modification temperature (Liu et al., 2022). Similarly, drying time showed a positive correlation with the flexural strength and compressive strength of MPG (Taplin, 2004). Through comparison, flexural strengths and compressive strength of PG at  $180^{\circ}\text{C}/7\text{ h}$ ,  $195^{\circ}\text{C}/7\text{ h}$  and  $195^{\circ}\text{C}/10\text{ h}$  can meet the requirements of GB/T9776, while the mechanical properties of PG at  $165^{\circ}\text{C}$  cannot meet the criteria (Singh and Middendorf, 2007).

##### 3.1.3. Softening coefficient

The softening coefficient reflects the water repellency of PG. From Fig. 10, the softening coefficient of MPG increases with the increase of temperature under the same holding time. The softening coefficient of PG at  $165^{\circ}\text{C}$  and  $180^{\circ}\text{C}$  increased obviously. The changing trend of softening coefficient of MPG from  $180^{\circ}\text{C}$  to  $195^{\circ}\text{C}$  is slight, but it also shows an increasing trend. It is generally believed that the material has better water resistance when the softening coefficient is more significant than 0.8 (Chen et al., 2022). In

**Table 7**

The standard consistency water consumption and setting time test of MPG.

NO.	Temperature (°C)	Holding time (h)	Standard consistency water consumption	Setting time (min)	
				Initial	Final
MPG	165	5	55%	4.50	5.20
	165	7	57%	5.00	9.00
	165	10	60%	3.00	4.00
	180	5	65%	5.50	6.20
	180	7	73%	3.25	4.10
	180	10	75%	5.00	6.40
	195	5	68%	6.10	6.50
	195	7	70%	5.40	7.10
	195	10	72%	6.20	8.10

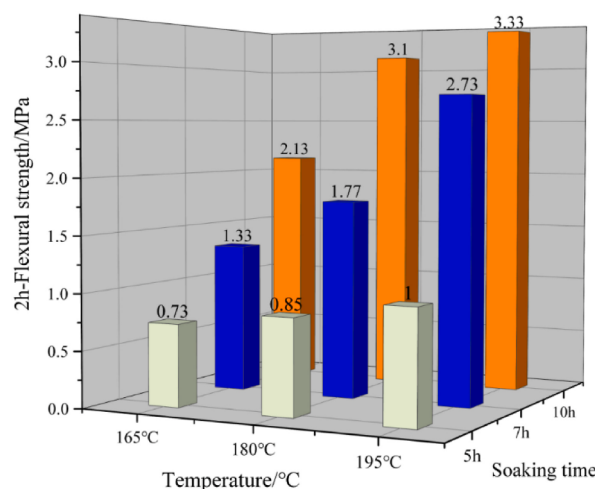


**Fig. 8.** MPG 2 h-bending strength.

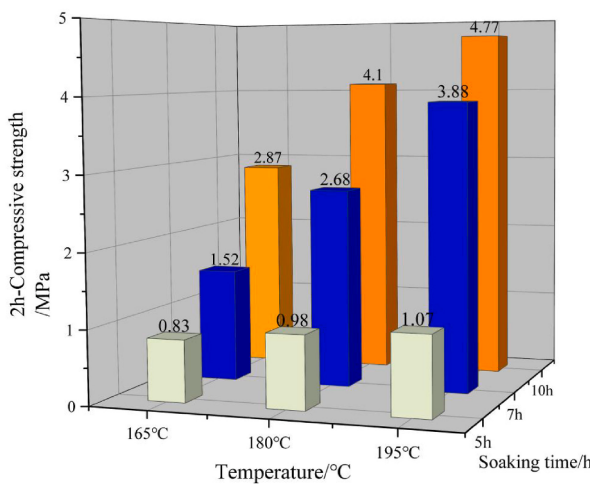


**Fig. 9.** MPG 2 h-compressive strength.

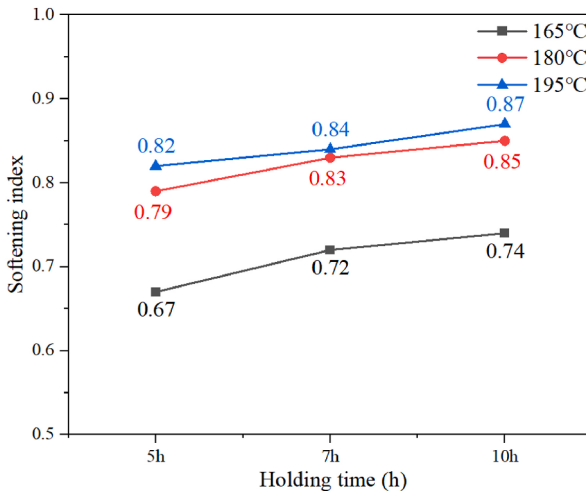


**Fig. 10.** The softening coefficient test result of MPG.

all data, under the test conditions of 165 °C, the softening coefficient of MPG can't meet the requirements GB/T9776 of greater than 0.8.

In conclusion from the analysis of the macroscopic properties of MPG, the MPG at 180 °C/10, 195 °C/7 h and 195 °C/10 h can meet the requirements of mechanical properties and setting time in the Chinese standard GB/T9776 (Level 2.0), and the appearance are closer to ordinary gypsum. The macroscopic properties each group of samples at 165 °C do not meet the standard of GB/T9776. All groups of MPG samples at 165 °C are discarded in the following analysis.

### 3.2. Microanalysis of thermodynamic modification mechanism

#### 3.2.1. XRD test results analysis and phase composition

Fig. 11 is the XRD pattern of six PG samples treated at different temperatures and holding times. The main minerals in PG are  $\text{CaSO}_4 \cdot m\text{H}_2\text{O}$  ( $m = 0, 0.5, 2$ ). The PG treated at 180 °C/5 h/7 h/10 h and 195 °C/5 h shows a strong diffraction peak at 11.588°. The most substantial diffraction peak at 11.588° is from  $\text{CaSO}_4 \cdot 2\text{H}_2\text{O}$ , the (020) crystal plane of  $\text{CaSO}_4 \cdot 2\text{H}_2\text{O}$  (Mi et al., 2018). Some MPG in 20.722°, 23.397° appeared  $\text{CaSO}_4 \cdot 2\text{H}_2\text{O}$  diffraction peak (Geraldo et al., 2020), with the increase of temperature and holding time,  $\text{CaSO}_4 \cdot 2\text{H}_2\text{O}$  diffraction peak gradually weakens until the peak disappeared (195 °C/7 h/10 h). Six kinds of MPG have diffraction peaks at 14.639, which belong to  $\text{CaSO}_4$ , and it is the (100) crystal form of  $\text{CaSO}_4$ . At the same holding time, the longer the holding time, the sharper the peak shape and the better the crystallization (Cao et al., 2021). Six kinds of MPG in 29.691° all appeared with diffraction peaks, the diffraction peak belongs to  $\text{CaSO}_4 \cdot 0.5\text{H}_2\text{O}$ , is  $\text{CaSO}_4 \cdot 0.5\text{H}_2\text{O}(400)$  crystal form, and the higher the temperature, the longer the holding time, the diffraction peak intensity gradually increased (Mittal and Rakshit, 2020). As can be seen from Table 8, when the calcination temperature is 180 °C, the content of gypsum dihydrate is related to the holding time in a negative way, while the content of gypsum hemihydrate is related to it in a positive way. The sample at 195 °C/5 h is dominated by  $\text{CaSO}_4 \cdot 0.5\text{H}_2\text{O}$  (77.56%). The content of  $\text{CaSO}_4 \cdot 0.5\text{H}_2\text{O}$  in the samples at 195 °C/7 h decreases obviously and

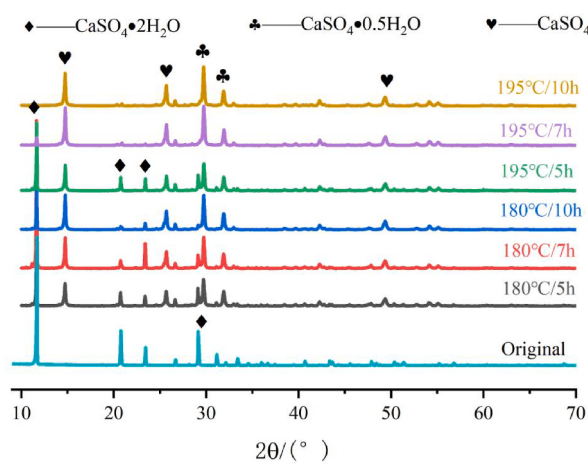


Fig. 11. XRD results of MPG.

**Table 8**  
Phase composition of MPG.

Temperature ( $^\circ\text{C}$ )	Holding time (h)	Phase composition		
		$\text{CaSO}_4 \cdot 2\text{H}_2\text{O}$	$\text{CaSO}_4 \cdot 0.5\text{H}_2\text{O}$	$\text{CaSO}_4$ (III)
180	5	31.27	30.62	0
180	7	26.10	32.24	8.15
180	10	20.49	75.07	20.03
195	5	16.23	77.56	3.01
195	7	23.45	49.11	20.62
195	10	7.28	55.76	28.59

the content of  $\text{CaSO}_4$  increases. The sample of  $195^\circ\text{C}/10\text{ h}$  is mainly  $\text{CaSO}_4$ . The intensity data indicated a positive effect of  $\text{CaSO}_4 \cdot 0.5\text{H}_2\text{O}$  and  $\text{CaSO}_4$  on MPG, which is consistent with the results of Liu et al.

### 3.2.2. FTIR analysis of MPG

The FTIR test results of MPG are depicted in Fig. 12. The peak at  $597\text{ cm}^{-1}$  corresponds to the Ca–O chemical bond formed by calcium ions and oxygen ions in MPG. Peaks at  $668\text{ cm}^{-1}$ ,  $1100\text{ cm}^{-1}$ , and  $1150\text{ cm}^{-1}$  are attributed to  $\text{SO}_4^{2-}$  ions (Xiang et al., 2023). The intensity of the  $\text{SO}_4^{2-}$  peak, serving as a fingerprint peak for assessing the purity of MPG, increases with higher calcination temperatures and prolonged holding times, indicating a more pronounced transformation of  $\text{CaSO}_4 \cdot 2\text{H}_2\text{O}$  to hemihydrate calcium sulfate.

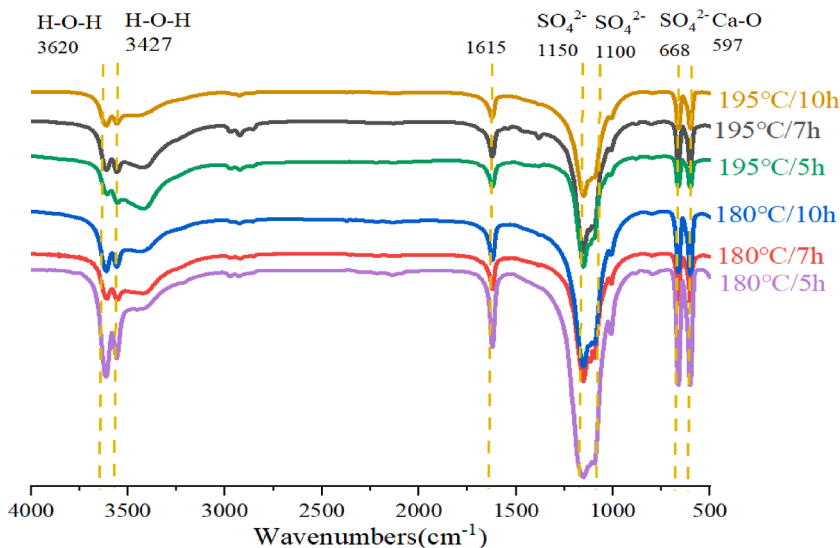


Fig. 12. The FTIR results of MPG.

The peak at  $1615\text{ cm}^{-1}$  represents the phosphorus impurity in MPG. Comparing the data in Fig. 12, it is evident that the intensity of the phosphorus impurity peak in MPG treated at  $195\text{ }^\circ\text{C}$  is significantly lower than that in MPG treated at  $180\text{ }^\circ\text{C}$ . This suggests that increasing the temperature is conducive to reducing phosphorus impurities in MPG. The peak in the range of  $3620\text{ cm}^{-1}$  to  $3427\text{ cm}^{-1}$  corresponds to the H–O–H peak caused by water ( $\text{H}_2\text{O}$ ) in MPG. The peak intensity decreases with the reduction in temperature and holding time, indicating a gradual decrease in moisture content in MPG.

### 3.2.3. SEM-EDS test results of MPG

**3.2.3.1. Analysis of powder MPG.** From Fig. 13, the PG is mainly plate-like or diamond-shaped structure with a size of  $30\text{--}40\text{ }\mu\text{m}$ . Fig. 14 shows that when the calcination temperature is  $180\text{ }^\circ\text{C}$ , the MPG crystal debris particles with a holding time of  $10\text{ h}$  are the most and the smallest particle size. When the calcination temperature reaches  $195\text{ }^\circ\text{C}$  and the holding time reaches  $10\text{ h}$ , MPG has the most layered and prominent cracks. When the holding time is  $5\text{ h}$ , the MPG crystal cracking degree is greater at  $195\text{ }^\circ\text{C}$ . When the holding time is  $7\text{ h}$ , the particle size of MPG at  $195\text{ }^\circ\text{C}$  is smaller. At  $195\text{ }^\circ\text{C}$ , there are more lamellar cracks in the MPG crystals, and the overlapping of the crystals in each layer is closer.

After modification (calcination), the overall aspect ratio of crystal particles in PG decreases, indicating a significant improvement in crystal quality. As depicted in Fig. 14a–c, the plate-like crystals begin to crack with the increase in calcination temperature, and surface cracks form layered crystals (Chen et al., 2022a). At  $180\text{ }^\circ\text{C}$ , the plate-shaped clustered crystals' surface begins to show signs of damage and cracks. As the cracks between the layers of crystals increase, the surrounding debris particles also increase. The larger the cracks between the crystals of each layer, the larger the surrounding debris particles. At  $185\text{ }^\circ\text{C}/10\text{ h}$ , the number of broken particles is the largest, and the debris particles are mainly composed of  $\text{CaSO}_4\cdot0.5\text{H}_2\text{O}$  and  $\text{CaSO}_4$ . The increase of small particles improves the compactness of the internal structure of PG, thereby improving the fluidity of PG products (Li and Zhang, 2021). From Fig. 14 d–f, the situation at  $195\text{ }^\circ\text{C}$  and  $180\text{ }^\circ\text{C}$  is roughly the same, but the microscopic morphology of  $195\text{ }^\circ\text{C}/10\text{ h}$  and  $180\text{ }^\circ\text{C}/10\text{ h}$  appears obvious changes, and the crystal shows obvious cracks. The dense parallelogram crystal becomes a layered parallelogram crystal, which is due to the production of  $\text{CaSO}_4\cdot0.5\text{H}_2\text{O}$  and  $\text{CaSO}_4$  phase. After the temperature modification of PG, the rate of crystal decomposition tends to increase and the particle size tends to decrease as the holding time increases at the same temperature. The degree of crystal decomposition becomes more complete as the temperature rises if the holding time remains constant. Through EDS analysis, it is found that the powdered MPG at  $185\text{ }^\circ\text{C}$  and  $190\text{ }^\circ\text{C}$  contained heavy metal elements such as Cr, As, Hg, Cd, etc. This may pose potential safety risks to the environment or human health. More accurate testing methods should be employed to study the content of heavy metals.

**3.2.3.2. Analysis of MPG after hydration.** The strength of PG depends on the crystal strength generated by hydration, the number of crystal contact points and the porosity of hardened body (Costa et al., 2022). Calcination causes the main components of PG to be transformed into calcium sulfate hemihydrate and anhydrous calcium sulfate. When the MPG is hydrated into gypsum block, its interior is mainly composed of long rod-like crystals. The crystals are crisscrossed, overlapped with each other or overlapped with some flake structures (Fig. 15). With the increase in holding time and temperature, there are more and more plate-like, short columnar and amorphous cementitious materials, and the crystals are closely connected (Huang et al., 2022). These amorphous colloidal substances are mainly  $\text{CaSO}_4\cdot2\text{H}_2\text{O}$  tiny crystals and a small number of impurities. Combined with the strength test results of Figs. 8–9, it can conclude that the increase of cementitious material can effectively improve the flexural and compressive strength of MPG.

### 3.2.4. Particle size distribution of powder MPG

The particle size distribution influences the solidification time of PG. Table 9 shows that the setting time of MPG at  $180\text{ }^\circ\text{C}$ – $195\text{ }^\circ\text{C}$  is less than  $30\text{min}$ , which meets the Chinese proposal of GB/T9776. The particle size of MPG at  $180\text{ }^\circ\text{C}$  for  $7\text{ h}$  is more minor, leading to the shorter initial and final setting times (Xie et al., 2022).

From Table 9 and Fig. 16, at  $195\text{ }^\circ\text{C}$ , the medium particle size (D50) of MPG decreases with the increase in drying time. This is mainly because with the increase of holding time, the dihydrate gypsum is partially dehydrated into hemihydrate gypsum, and the larger particles are gradually decomposed, resulting in the gradual shortening of its setting time.

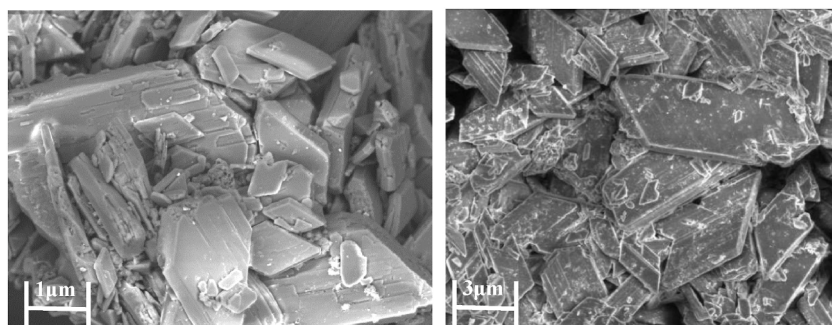


Fig. 13. PG SEM image.

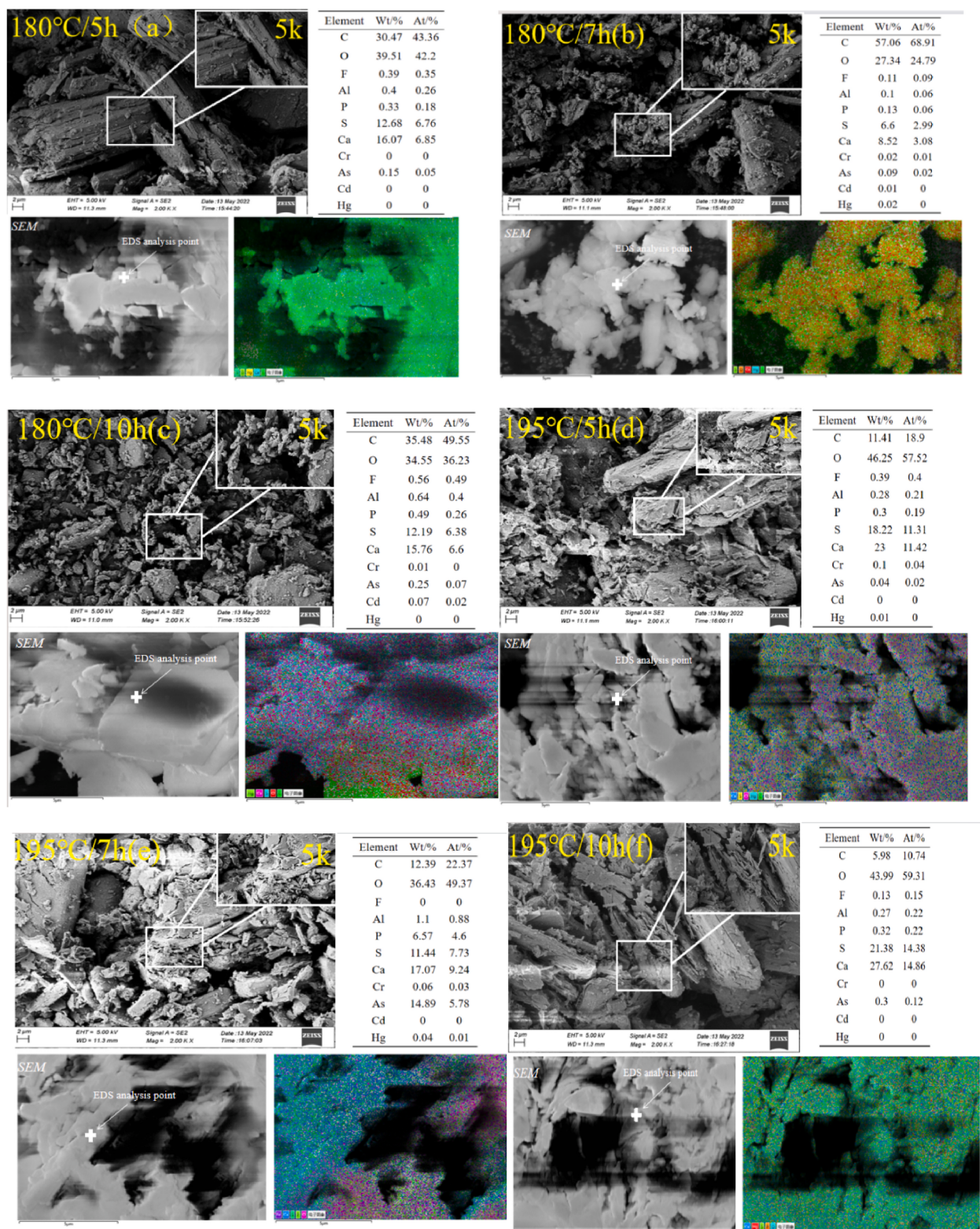


Fig. 14. Powder MPG SEM-EDS image.

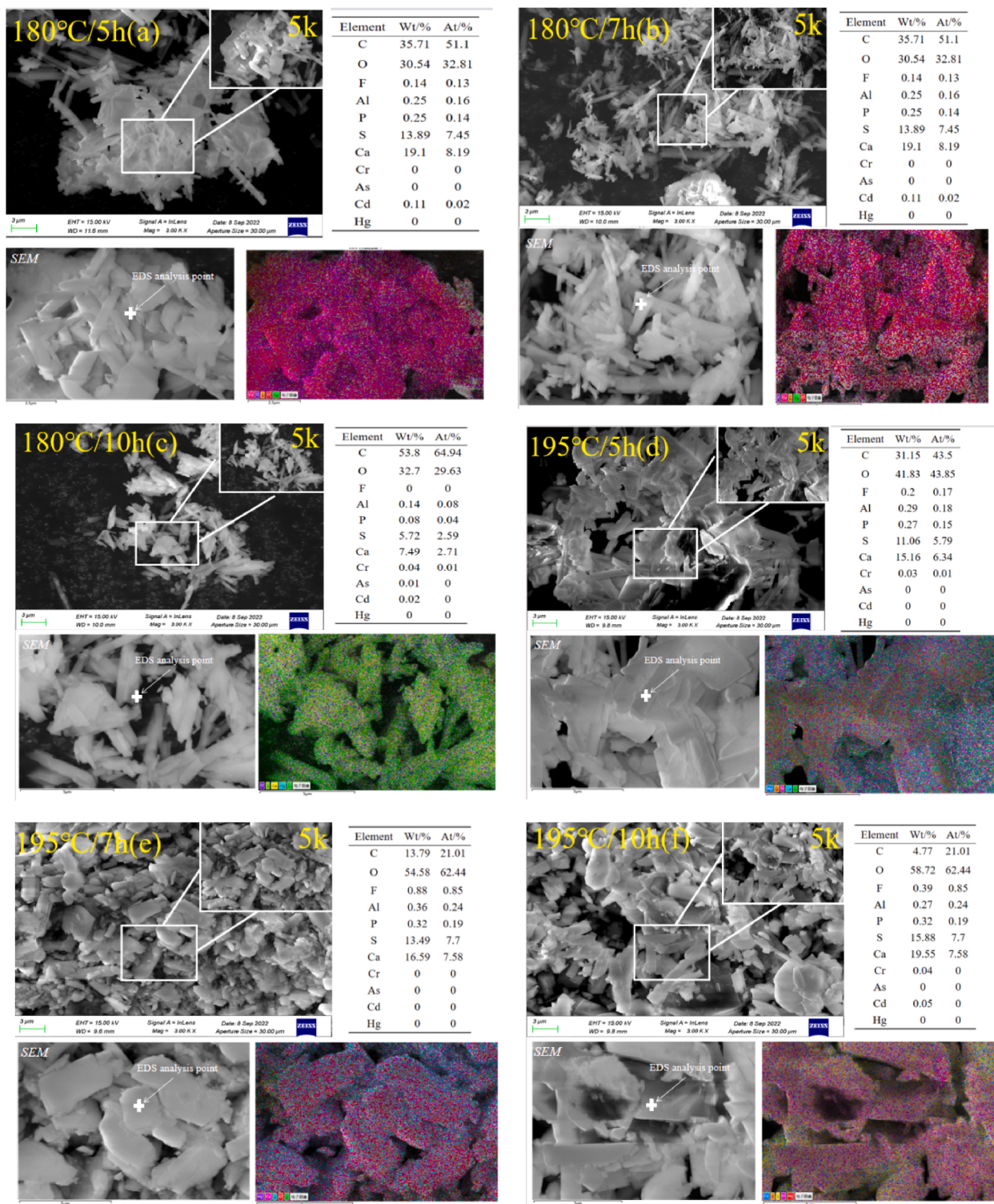


Fig. 15. SEM-EDS diagram of MPG after hydration.

### 3.3. The fate of heavy metals in MPG

Heavy metals and other impurities in PG will migrate in soil, water, and the atmosphere, threatening human health (Li et al., 2018). An in-depth study of the coupling mechanism of characteristic heavy metals in PG is significant for reducing its environmental pollution risk, improving human health and living indicators, and promoting its high-value application (Wang et al., 2022). Accord-

**Table 9**  
Setting time and particle size of MPG.

NO.	D (10)	D (50)	D (90)	
MPG	180 °C/5 h	2.9	20.7	54.7
	180 °C/7 h	1.5	7.5	32.0
	180 °C/10 h	1.6	9.2	38.5
	195 °C/5 h	1.5	7.3	33.2
	195 °C/7 h	1.3	6.1	31.8
	195 °C/10 h	1.2	4.9	24.7

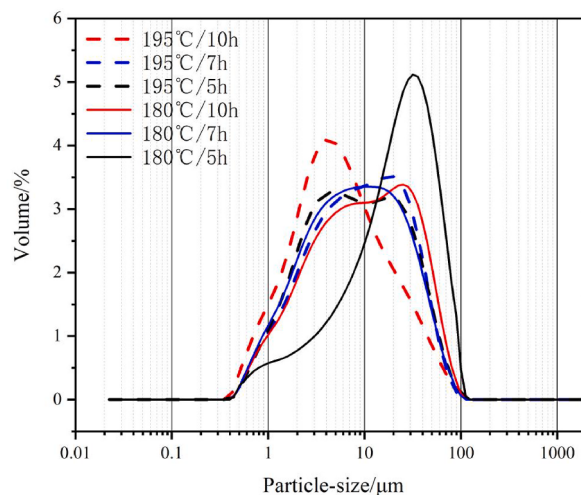


Fig. 16. Powder MPG particle size test results.

ing to the previous studies of the research group and other experts (Al-Hwaiti et al., 2019; Yelatontsev and Mukhachev, 2021; Wang et al., 2023), the primary hazardous heavy metals in PG are Cr, As, Cd and Hg. Hence, this study examines the levels of heavy metal elements in PG, MPG, and hydrated MPG. The leaching test results are used to analyze the leaching mechanisms of heavy metals.

### 3.3.1. Analysis of heavy metal content in PG/MPG

As shows in Table 10, the content of Cr in PG is the highest, reaching 31 mg/kg. Cd is 3.28 mg/kg, 11 times the standard value. The heavy metal values of calcined ground and hydrated PG have been markedly reduced. Among them, Cd has been reduced to a safe range, and significant decreases in Cr, Cd, and Hg have been observed.

### 3.3.2. The heavy metals fate from PG to powder MPG

As shown in Table 10, the Cr element decreased from the PG 31 mg/kg to about 1.50mg/kg, and the decrease rate was as high as 95%. The As element decreased from 2.77 mg/kg to 0.05–0.86 mg/kg, and the lowest decrease rate in the MPG at 180 °C/10 h reached 80%. The content of Cd decreased from 3.28 mg/kg to 0.1–0.3 mg/kg, and the decreasing ratio reached 99%. The content of Hg decreased from 0.06 mg/kg to 0.01 mg/kg, and the decreasing rate reached 83%. The reasons for the decrease of heavy metals in MPG during the process from PG to powder MPG can be explained from three aspects.

Examining the conversion of heavy metal ions in Fig. 17, the temperature-treated PG undergoes a transformation from  $\text{CaSO}_4 \cdot 2\text{H}_2\text{O}$  to a mixture of  $\text{CaSO}_4 \cdot m\text{H}_2\text{O}$  ( $m = 0, 0.5, 2$ ). This transformation, as highlighted by Peng et al. (2021), induces a significant alteration in the crystal development within the PG. Simultaneously, the van der Waals force of the molecular bond and the covalent bond between ions are disrupted, initiating a replacement process. Calcium sulfate dihydrate, categorized within the monoclinic system, sees  $\text{SO}_4^{2-}$  tetrahedra and  $\text{Ca}^{2+}$  ions linking into a double-layer structure parallel to the (010) plane. Between these double lay-

**Table 10**  
Heavy metal leaching content in PG and MPG (mg/kg).

NO.	PG	Original	Gr	As	Cd	Hg
			31.00	2.77	3.28	0.06
After calcination	MPG	180 °C/10 h	1.47	0.56	0.02	0.01
		195 °C/10 h	1.51	0.86	0.03	0.01
After hydration		180 °C/10 h	1.44	0.93	0.01	0.00
		195 °C/10 h	1.42	1.95	0.13	0.00
Standard value	GB15618		150	30	0.3	0.5

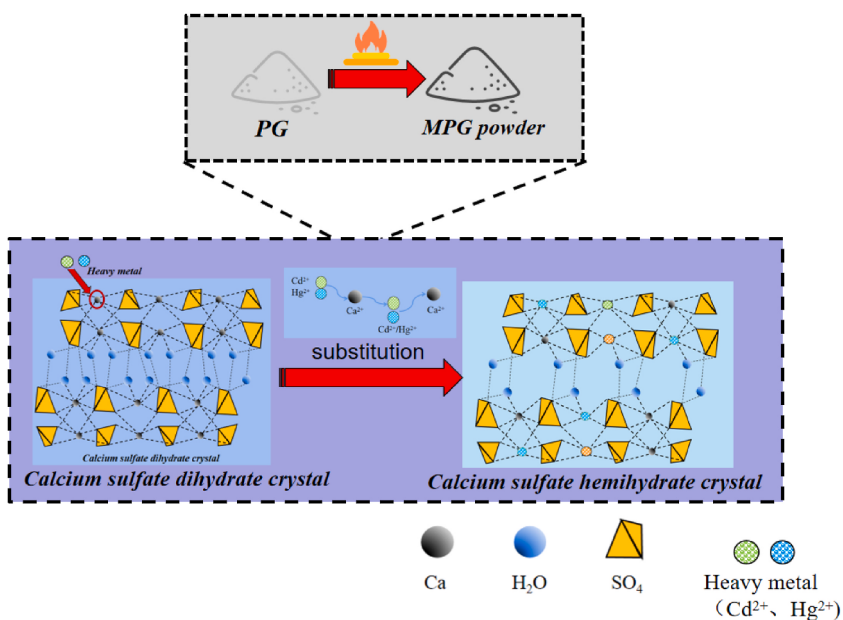


**Fig. 17.** Heavy metal ion replacement mechanism diagram (Calcium sulfate dihydrate in the calcination process to form calcium sulfate hemihydrate replacement of heavy metals as an example).

ers,  $\text{H}_2\text{O}$  molecules are distributed. The coordination number of  $\text{Ca}^{2+}$  is 8, with  $\text{Ca}^{2+}$  bound to six  $\text{O}^{2-}$  ions in four adjacent  $\text{SO}_4^{2-}$  tetrahedra and two water molecules. A hydrogen bond connects the water molecule with  $\text{O}^{2-}$  in  $\text{SO}_4^{2-}$ , while water molecules are interconnected by molecular bonds (Massaro et al., 2010). On the other hand, calcium sulfate hemihydrate, part of the monoclinic system (Zarei et al., 2021), exhibits a layered structure parallel to the (100) and (010) planes, formed by the linkage of  $\text{SO}_4^{2-}$  tetrahedra and  $\text{Ca}^{2+}$  ions. The theory influencing ion radius on heavy metal replacement encompasses the Houm-Rathery law (Komarneni et al., 1988) (i.e., the 15% volume-mismatch allowable error law) and the Vigard theorem (Zhou, Y. et al., 2022). These theories respectively delineate the limitations of ion radius gaps and the correlation between changes in lattice parameters of solid solutions and the radius of impurity ions during substitution. The alteration in the average lattice constant of the crystal during the formation of the substitutional solid solution is contingent upon the relative size of the impurity ion radius and the matrix ion radius. Formation of the interstitial solid solution leads to an increase in the average lattice constant of the crystal. The size of the added atoms is intricately related to the lattice structure, and ions added to the gap position must be balanced by charges to maintain electrical neutrality. The radius difference of  $\text{Cr}^{3+}$ ,  $\text{Cr}^{6+}$ ,  $\text{As}^{3+}$ ,  $\text{As}^{5+}$ ,  $\text{Cd}^{2+}$ ,  $\text{Hg}^{2+}$ , and the polarization ability of these ions were calculated based on the Houm-Rathery law and Vigard theorem.

The ionic radius of each element is shown in Table 11. The difference between the radii of  $\text{Cd}^{2+}$  and  $\text{Hg}^{2+}$  and  $\text{Ca}^{2+}$  is less than 15%, so these two ions can replace the hemihydrate or anhydrous calcium sulfate  $\text{O}^{2-}$  and the octahedral  $\text{Ca}^{2+}$  to form a displacement solid solution (Stephan et al., 1999). The radius difference between  $\text{Cd}^{2+}$ ,  $\text{Hg}^{2+}$  and  $\text{Ca}^{2+}$  is less than 15%, so these two ions can replace half-water or anhydrous calcium sulfate  $\text{O}^{2-}$  to form a replacement solid solution (Stephan et al., 1999).  $\text{As}^{3+}$  and  $\text{Cr}^{3+}$  are easily replaced by  $\text{Fe}^{3+}$  to form a substitutional solid solution, which also satisfies the theoretical knowledge that ions of the same valence state can be replaced and form a solid solution (Tanabe and Takeshita, 1967). The ionic radius of  $\text{As}^{5+}$  in MPG does not meet the Houm-Rathery law. However previous studies have shown that (Miroslav et al., 2021),  $\text{As}^{5+}$  can form a bidentate mononuclear complex with  $\text{Fe}^{3+}$ , thereby reducing the leaching amount. A semi-quantitative analysis through SEM-EDS reveals that the concentrations of Ca and Fe in powdered MPG at 180 °C/10 h are lower compared to those at 195 °C/10 h. This observation supports the confirmation that Ca and Fe undergo substitution reactions with heavy metals such as Cd, Hg, As, and Cr during the modification process.

**Table 11**  
Element ion radius parameters.

Ionic species	Peripheral electron configuration	Ionic radius (pm)	Coordination number	Electronegativity	Radius difference with $\text{Ca}^{2+}$ ( $(R_n - R_{\text{Ca}})/R_{\text{Ca}}$ )	Radius difference with $\text{Fe}^{3+}$ ( $(R_n - R_{\text{Fe}})/R_{\text{Fe}}$ )
$\text{Ca}^{2+}$	4s2	100	6	1.04	/	/
$\text{Fe}^{3+}$	3d64s2	65.4	6	1.64	/	/
$\text{Cr}^{3+}$	3d54s1	61.5	6	1.56	-38.50%	-5.96%
$\text{Cd}^{2+}$	3d105s2	95.0	6	1.46	-5.00%	45.26%
$\text{Hg}^{2+}$	5d106s2	102.0	4	2.00	2.00%	55.96%
$\text{As}^{3+}$	4s24p3	58.0	6	2.20	-42.00%	-11.31%
$\text{As}^{5+}$	4s24p3	46.0	10	2.20	-54.00%	-29.66%

From the aspect of modification temperature, under the modification condition of 180 °C/10 h, Cr and As elements are slightly lower than that of 195 °C/10 h, mainly because the crystal properties have a greater impact on heavy metal adsorption. In forming the crystal form of hemihydrate gypsum, the larger specific surface area of hemihydrate gypsum has a greater adsorption effect. As shown in Fig. 18 and Fig. 19, the MPG particles at 180 °C/10 h are smaller and have a larger specific surface area, which leads to

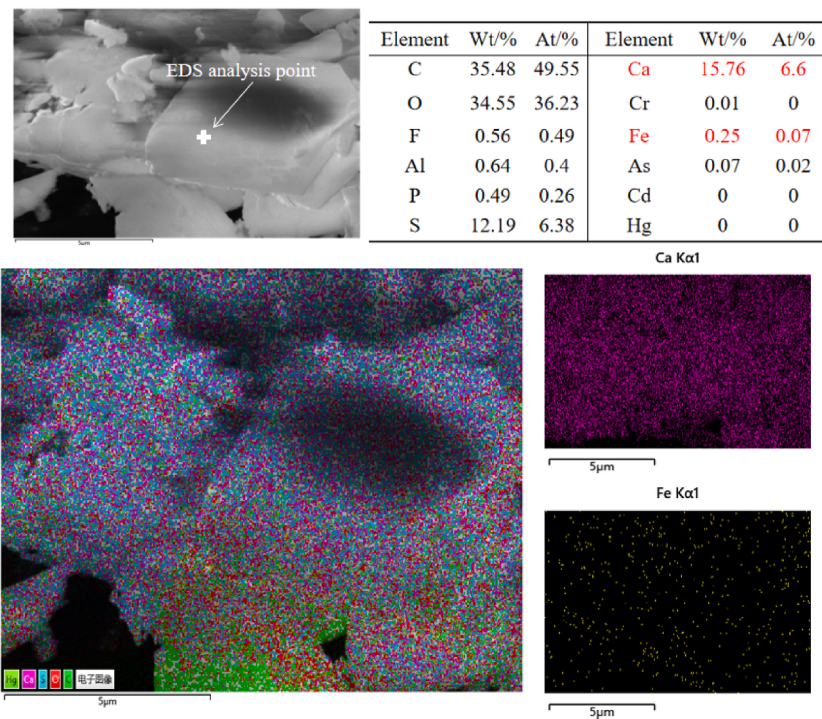


Fig. 18. SEM-EDS spectrum of powdered MPG at 180 °C/10 h

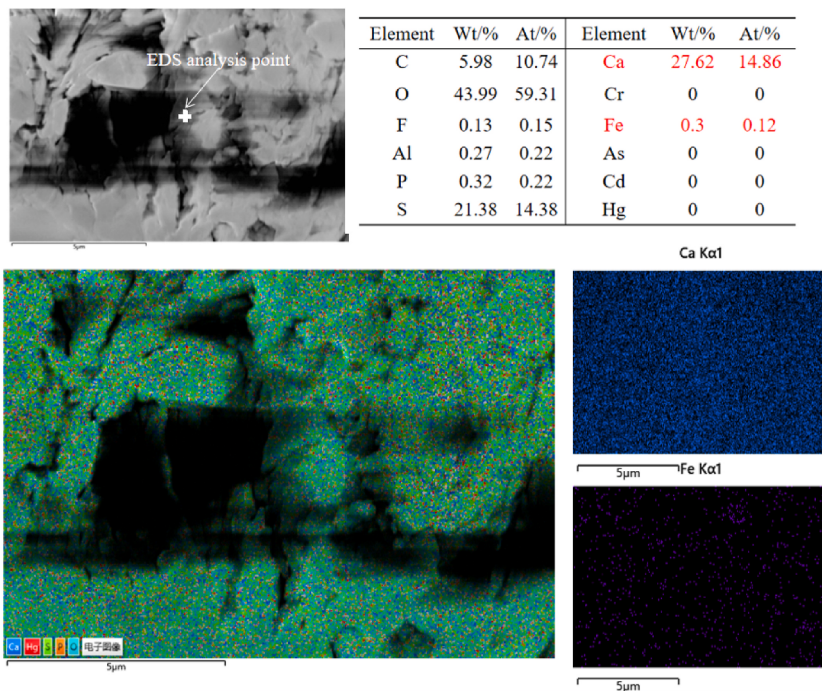


Fig. 19. SEM-EDS spectrum of powdered MPG at 195 °C/10 h

stronger adsorption. **Table 8** phase composition of MPG can also be clearly observed in the 180 °C/10 h content of hemihydrate gypsum than other components.

Analysis of the causes of heavy metal reduction from the perspective of grinding methods (He et al., 2022; Nomura et al., 2008). The original appearance of PG is characterized by large block-like structures. In this experiment, grinding was conducted using a mill, as illustrated in **Fig. 20**. The samples must meet the requirements of the Chinese standard GB/T 9776. Previous studies have indicated that ball milling can result in a rougher sample surface, reduced particle size, increased pore volume, average pore diameter, and specific surface area (Sun et al., 2011; Wu et al., 2013). The pore structure becomes more diverse, with a noticeable increase in the number of large and medium-sized pores, thereby enhancing the solidification capacity of the solid waste for heavy metals.

### 3.3.3. The heavy metals fate in MPG from powder to hydration

The mechanism of gypsum hydration has been widely studied at home and abroad. The hydration mechanism of gypsum is mainly divided into two kinds, one is dissolution crystallization theory, and the other is colloid theory. According to the dissolution crystallization theory, the solubility of hemihydrate gypsum in water is highly saturated relative to dihydrate gypsum, and dihydrate gypsum spontaneously crystallizes until the hemihydrate gypsum is completely hydrated to form dihydrate gypsum (Chen et al., 2022b). Colloid theory suggests that the hydration process of gypsum is similar to the hydration process of cement and that after hemihydrate gypsum or anhydrite is stirred with water, water forms a gel in the solid phase of hemihydrate gypsum, through which a needle-like crystal, namely dihydrate gypsum, is presented (Follner et al., 2002). Nevertheless, there are few studies on the changes of heavy metals in the hydration process of PG in China and abroad. From **Table 10**, the content of the Cr element after hydration is lower than that of the powder. The decrease of 195 °C/10 h reached 0.09 mg/kg. The minimum decrement was 0.03 mg/kg at 180 °C/10 h. The reason for the low drop at 180 °C/10 h is that the heavy metal content of MPG is limited. The number of heavy metals in powdered MPG treated at 180 °C/10 h decreased the most, which led to the decrease of Cr after hydration, which was lower than that of the other two groups.

The content of Hg was also significantly lower than that of powdered heavy metals, reaching 0 mg/kg. It shows that the harm of Hg element in PG to environment can be completely removed by low temperature calcination, grinding, and hydration process. The calcium sulfate dihydrate gel has a certain adsorption effect on Cr and Hg, which leads to the further decrease of the two heavy metal elements in the hydration process (**Fig. 21**). The pH value of the MPG after High efficiency calcination is between 6.1 and 7.0, showing weak acidity or alkalinity, while As is mainly  $\text{H}_2\text{AsO}_4^-$  in weak acidity or alkalinity (Lopes et al., 2013). When the content of  $\text{Ca}^{2+}$  is high,  $\text{H}_2\text{AsO}_4^-$  can react with  $\text{Ca}^{2+}$  as follows:  $\text{Ca}(\text{H}_2\text{AsO}_4)_2$ . As the detection method of heavy metal concentration is based on the Chinese standard of "Solid waste leaching toxicity leaching method sulfuric acid nitric acid method" (HJ/T299), and  $\text{Ca}(\text{H}_2\text{AsO}_4)_2$  is slightly soluble in water and easily soluble in acid, the leaching amount of As element after hydration is higher than that of powder. The increase in Cd is due to the reductive dissolution of iron oxides contained in MPG at the initial hydration stage (Kashem and Singh, 2001).



### 3.4. Safety assessment of hydration MPG

Some of the heavy metals in MPG are highly ecologically hazardous (Fatoki and Badmus, 2022; Wang, 2020). In this study, four risk assessment models are used to investigate the ecological safety of heavy metals contained in PG and MPG after hydration.

#### 3.4.1. Single factor index method

The single factor index evaluation results of PG/MPG in **Table 12** show that the Pi value of Cd element is 10.93, which has serious environmental safety risks. Pi values for all other elements do not exceed 0.5. The single factor pollution index of Cr, As, Cd and Hg in

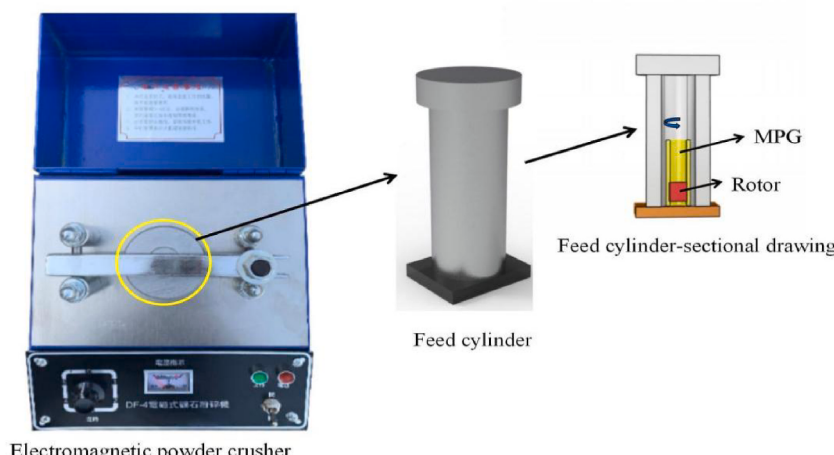


**Fig. 20.** Electromagnetic crushing activation of heavy metals schematic diagram.

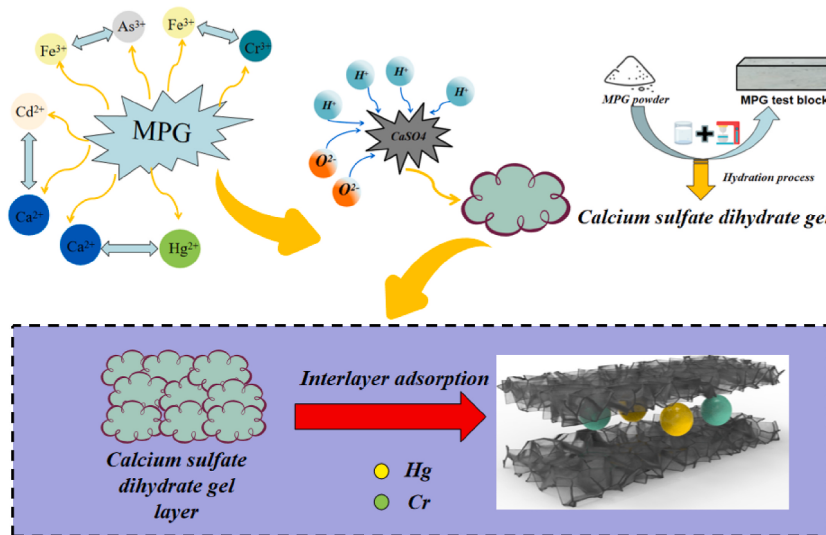


Fig. 21. Schematic diagram of heavy metals wrapped in  $\text{CaSO}_4 \cdot 2\text{H}_2\text{O}$  during hydration.

**Table 12**  
Heavy metal pollution index (mg/kg).

NO.	$P_i$			
	Cr	As	Cd	Hg
PG	0.21	0.09	<b>10.93</b>	0.12
180 °C/10 h	0.01	0.03	0.03	–
195 °C/10 h	0.01	0.07	0.43	–

MPG is less than 0.5, which belongs to non-pollution. It is judged by single factor index method that heavy metals in MPG do not pollute the environment.

### 3.4.2. Potential ecological risk index method

From Table 13, the environmental potential ecological risk level (RI) value of the four heavy metal elements in the PG is 11.57, L (Low risk). The Hg element in the  $E_i$  value reached 8.00. The  $E_i$  value of Cr is 1.24, the  $E_i$  value of As is 0.92, and the  $E_i$  value of Cd is 1.41. Compared with other heavy metal elements, Hg has certain environmental safety risks. The  $E_i$  and RI values of MPG were significantly reduced, so there was no environmental hazard.

### 3.4.3. Geological accumulation index method

For this PG, the  $I_{ego}$  of Hg is 3.69, which is a serious pollution level, while Cd, Cr and As are pollution-free. The  $I_{ego}$  index of MPG is negative, and there is no environmental safety risk in Table 14.

### 3.4.4. Human health risk assessment

**3.4.4.1. Non-carcinogenic risk.** From Table 15, the non-carcinogenic risks of PG and MPG are in line with the standard of  $HI < 1$  stipulated by US EPA, and there was no non-carcinogenic risk.

**3.4.4.2. Carcinogenic risk.** Table 16 shows the total carcinogenic risk index of PG and MPG by mouth-mouth intake, respiratory intake and skin contact. The results showed that the total carcinogenic risk of oral-to-hand ingestion of PG and MPG is within the acceptable carcinogenic risk range for kids and grown-ups ( $10^{-4} < TCR < 10^{-6}$ ), and the total carcinogenic risk for kids is considerably more significant than that for grown-ups. Through the study of three different carcinogenic risks of PG and MPG in Tables 16–19, it

**Table 13**  
Potential ecological risk index of heavy metals in PG and MPG.

NO.		Cr	As	Cd	Hg	RI
PG	$E_i$	1.24	0.92	1.41	<b>8.00</b>	11.57
	Ecological grade	E	E	E	E	L
180 °C/10 h	$E_i$	0.06	0.31	–	–	0.37
	Ecological grade	E	E	–	–	L
195 °C/10 h	$E_i$	1.42	0.65	0.06	–	0.76
	Ecological grade	E	E	E	–	L

**Table 14**  
 $I_{geo}$  of PG under different pretreatment conditions.

NO.		Cr	As	Cd	Hg
PG	$I_{geo}$	-2.06	-2.74	<b>3.69</b>	-1.17
	Class	0	0	<b>4</b>	0
	Degree	N	N	<b>H</b>	N
180 °C/10 h	$I_{geo}$	-6.49	-4.31	-4.67	-
	Class	0	0	0	-
	Degree	N	N	N	-
195 °C/10 h	$I_{geo}$	-6.54	-3.24	-0.97	-
	Class	0	0	0	-
	Degree	N	N	N	-

**Table 15**  
HI of PG/MPG under different intake pathways.

NO.	PG	180 °C/10 h		195 °C/10 h	
		Grown-up	Kid	Grown-up	Kid
HI <sub>ing</sub>	2.77E-01	6.47E-01	3.02E-03	2.98E-03	1.88E-03
HI <sub>inh</sub>	1.58E-06	4.82E-06	1.07E-07	3.28E-07	1.53E-07
HI <sub>der</sub>	3.36E-04	5.50E-04	4.45E-06	7.28E-06	7.72E-06
Total	2.78E-01	6.48E-01	3.02E-03	2.98E-03	1.88E-03
					4.39E-03

**Table 16**  
TCR of PG/MPG under different intake pathways.

NO.	PG	180 °C/10 h		195 °C/10 h	
		Grown-up	Kid	Grown-up	Kid
TCR <sub>ing</sub>	<b>9.90E-05</b>	<b>2.31E-04</b>	<b>5.41E-06</b>	<b>1.26E-05</b>	<b>6.46E-06</b>
TCR <sub>inh</sub>	5.39E-10	1.65E-09	2.97E-11	9.07E-11	5.04E-11
TCR <sub>der</sub>	7.09E-08	1.16E-07	6.07E-09	9.94E-09	9.64E-09
Total risk	<b>9.91E-05</b>	<b>2.31E-04</b>	<b>5.41E-06</b>	<b>1.26E-05</b>	<b>6.47E-06</b>
					<b>1.51E-05</b>

**Table 17**  
CR of selected heavy metals under oral intake conditions.

NO.	PG	180 °C/10 h		195 °C/10 h	
		Grown-up	Kid	Grown-up	Kid
Cd (CR <sub>ing</sub> )	<b>1.50E-06</b>	<b>3.50E-06</b>	4.57E-09	1.07E-08	4.57E-09
Cr (CR <sub>ing</sub> )	<b>9.45E-05</b>	<b>2.21E-04</b>	<b>4.39E-06</b>	<b>1.02E-05</b>	<b>4.33E-06</b>
As (CR <sub>ing</sub> )	<b>3.02E-06</b>	<b>7.04E-06</b>	<b>1.01E-06</b>	<b>2.36E-06</b>	<b>2.12E-06</b>
					<b>4.96E-06</b>

**Table 18**  
CR of selected heavy metals under inhalation conditions.

NO.	PG	180 °C/10 h		195 °C/10 h	
		Grown-up	Kid	Grown-up	Kid
Cd (CR <sub>inh</sub> )	2.72E-10	8.31E-10	8.28E-13	2.53E-12	8.28E-13
Cr (CR <sub>inh</sub> )	2.10E-10	6.44E-10	9.78E-12	2.99E-11	9.64E-12
As (CR <sub>inh</sub> )	5.68E-11	1.74E-10	1.91E-11	5.83E-11	4.00E-11
					<b>1.22E-10</b>

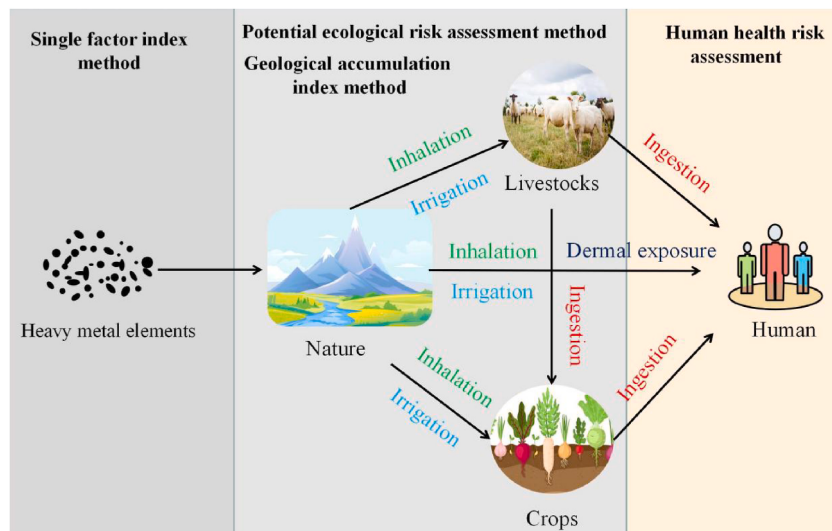
was found that the risks of As, Cd, Cr in PG to kids and grown-ups exceeded the standard of the US EPA, which was the reason for the high TCR value. The elements of As and Cd in the other two groups of MPG samples were high, resulting in the CR value of the oral single intake pathway within the acceptable carcinogenic risk range. Therefore, the supervision of Cr and As element content should be strengthened during the MPG pretreatment process, while the protection of workers' hands and faces should be enhanced during the treatment process to ensure workers' safety.

Through the above analysis of various environmental safety and human health risk models, it is found that Hg in PG has an environmental safety risk in single factor index method and potential ecological risk assessment method. Cd has environmental safety risk in geological accumulation index method, and MPG has no environmental safety risk. The results showed an acceptable range of carcinogenic risks to kids and grown-ups from the oral intake pathway in the PG and MPG. Fig. 22 is a schematic diagram of the process

**Table 19**

CR of selected heavy metals under dermal contact conditions.

NO.	PG	180 °C/10 h		195 °C/10 h	
		Grown-up	Kid	Grown-up	Kid
Cd (CR <sub>der</sub> )	1.20E-09	1.97E-09	3.67E-12	6.01E-12	3.67E-12
Cr (CR <sub>der</sub> )	5.99E-08	9.80E-08	2.78E-09	4.55E-09	2.74E-09
As (CR <sub>der</sub> )	9.79E-09	1.60E-08	3.29E-09	5.38E-09	6.89E-09
					1.13E-08

**Fig. 22.** Illustration of the process of heavy metal action on the ecosystem.

of heavy metals in PG affecting the ecosystem. The figure shows that the influence of heavy metal elements in PG on environmental safety and human health and safety is multi-channel and multi-faceted. Therefore, the monitoring of the characteristic heavy metal content in PG should be strengthened in conjunction with the resourceful use of PG, and the heavy metal limits for the different utilization stages of PG should be proposed.

### 3.5. Heavy metal limits for MPG in different applications

The results of the above analysis show that the rational use of PG should be accompanied by extra attention to the harmful effects of the heavy metals present. This study, based on relevant Chinese standards and legal regulations, employs the single-factor index method, potential ecological risk index method, geological accumulation index method, and human health risk assessment method to establish the maximum allowable concentrations of heavy metals in different scenarios. The specific results are presented in Table 20.

#### 3.5.1. Roads

When PG is applied to road base materials, the heavy metals in it can undergo leaching behaviour in response to external environmental effects such as rain, wheel loads and temperature. Therefore, based on the Chinese standard of GB15618 and "Soil environmental quality Risk control standard for soil contamination of development land" (GB36600). In this research, the limits for characteristic heavy metals for the use of MPG in road base materials are considered to be: As < 0.35 mg/kg and Cd < 0.12 mg/kg.

#### 3.5.2. Agriculture

PG is often used in agricultural production because of its special functions such as improving soil acidity and alkalinity and replenishing nutrients such as P and S. Therefore, for the application of PG in agriculture, the content of characteristic heavy metals should

**Table 20**

The heavy metal control values of MPG in different scenarios (mg/kg).

Application scenario	heavy metals	Limit value
Roads	As	< 0.35
	Cd	< 0.12
Agriculture	As	< 0.30
	Cd	< 0.10
Buildings	As	< 0.25
	Cd	< 0.08

be controlled. According to the Chinese standard of "Determination of arsenic, cadmium, chromium, lead and mercury contents for fertilizers" (GB/T23349), and GB36600, the heavy metal test results of MPG, the analysis results of this research, it is comprehensively proposed that the use of MPG materials in agriculture should meet: As < 0.30 mg/kg and Cd < 0.10 mg/kg.

### 3.5.3. Building materials

PG is widely used in construction materials because of its own gelling activity. According to the Chinese standard of "Quality standards for Phosphogypsum and its integrated utilization products" (DB4205/T063) and the analysis results of this research, it is comprehensively proposed that the use of MPG materials in building should meet: As < 0.25 mg/kg and Cd < 0.08 mg/kg.

## 3.6. MPG powder is used for PBSLM

### 3.6.1. Basic mechanical properties of PBSLM

The effects of MPG and cement content on the 0min/30min fluidity, 24 h-flexural, and compressive strength of PBSLM were investigated in Fig. 23 (a-d).

As exhibited in Fig. 23 (a), the initial 0-min and 30-min fluidity of PBSLM decrease with the increase of MPG content, from 150 mm to 153 mm of PBSLM1 to 145 mm and 149 mm of PBSLM3. The fluidity of PBSLM mainly depends on the friction resistance between quartz sand and the cohesion of PG. With the increase of MPG content, the cohesion of MPG hydration in PBSLM increases, resulting in a decrease in fluidity. As exhibited in Fig. 23 (b), when the MPG content is constant, with the decrease of cement content, the initial fluidity and 30 min flow of PBSLM increase, from 145 mm to 149 mm of PBSLM3 to 150 mm and 154 mm of PBSLM6. According to the author's analysis, the reasons for this phenomenon mainly depend on two aspects. On the one hand, cement will affect the hydration reaction process of gypsum. After a large amount of cement is dissolved in water, a large amount of  $\text{Ca}^{2+}$  and  $\text{OH}^-$  are rapidly generated (Dogan et al., 2022). The presence of  $\text{Ca}^{2+}$  is conducive to the chemical equilibrium of  $\text{Ca}^{2+} + \text{SO}_4^{2-} + 2\text{H}_2\text{O} \rightarrow \text{CaSO}_4 \cdot 2\text{H}_2\text{O}$  moving to the right, which promotes the formation of dihydrate gypsum (Li et al., 2020). On the other hand, too much cement content will affect the effect of retarder. The retarder forms a complex with  $\text{Ca}^{2+}$ , and the stability of the complex is related to pH. Under acidic and robust alkaline conditions, the stability of the complex is poor, and the retarding effect is reduced. Research indicates a significant relationship between the cement content and the quantity of ettringite generated, wherein a higher cement content results in a lower quantity of ettringite formed. As the proportion of cement in the entire system is relatively small, the

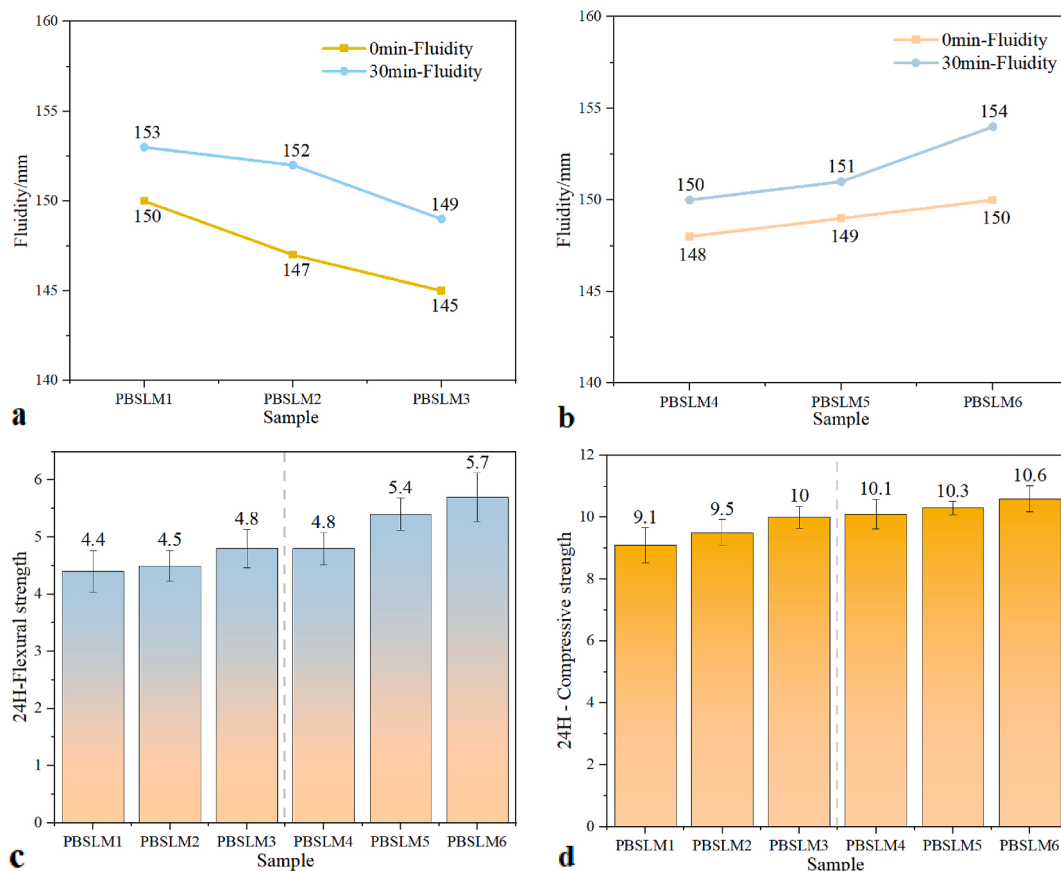


Fig. 23. The 0min/30min fluidity (a,b), 24 h-flexural and compressive strength (c,d) of PBSLM.

reduced quantity of ettringite generated has a minor impact on the overall setting time. Therefore, it can be disregarded (Sagitha et al., 2021; Zhang et al., 2020; Zhi et al., 2017).

Fig. 23(b and c) show PBSLM's 24 h-flexural and compressive strength. With the increase of PG content, the flexural and compressive strength of PBSLM have been improved. The flexural and compressive strength increased from 4.4 MPa to 9.0 MPa of PBSLM1 to 4.8 MPa and 9.95 MPa of PBSLM3, respectively. This is because the strength of the PG hardened body is mainly provided by the rigid skeleton structure formed by the overlapping of  $\text{CaSO}_4 \cdot 2\text{H}_2\text{O}$  crystals formed by the hydration of  $\text{CaSO}_4 \cdot 2\text{H}_2\text{O}$  (Zhang et al., 2018). The more MPG content, the denser the skeleton structure, which leads to an increase in strength.

Therefore, it can be concluded that the mechanical properties of PBSLM are optimal when the MPG dosage is 330 g. PBSLM3-4 investigated the trend of changes in the mechanical properties of PBSLM with the reduction of cement dosage when the MPG dosage is 330 g. It is not difficult to find that the strength of PBSLM has increased with the decrease in cement content. This mainly considers that in terms of early strength, when the cement content is high,  $\text{C}_3\text{A}$  in the cement will react rapidly with gypsum to form ettringite, which will limit the hydration of the cement.

The above analysis depicted that the mechanical properties of the PBSLM6 sample are optimal and also meet the requirements of the Chinese standard "Gypsum-based Self-leveling Mortar" (JC/T1023). Table 21 shows a comparison of the mechanical properties of the PBSLM6 sample with the standard values.

### 3.6.2. MPG powder used for gypsum-based self-leveling mortar microstructure

**3.6.2.1. XRF and XRD analysis.** Table 22 is the XRF analysis results of PBSLM6 sample. It can be found from the table that the main chemical elements of PBSLM6 sample are  $\text{SO}_3$ ,  $\text{CaO}$  and  $\text{SiO}_2$ , and the total amount of the three is more than 90%. As illustrated in Fig. 24, the PBSLM6 is mainly composed of  $\text{CaSO}_4 \cdot 2\text{H}_2\text{O}$ , which contains a small amount of  $\text{SiO}_2$  peaks introduced by sand and C-S-H and AFt peaks caused by cement hydration (Beldjilali et al., 2020).

**3.6.2.2. FT-IR analysis.** Fig. 25 is the FT-IR of PBSLM6 as a supplement to the XRD and XRF test results. There are seven characteristic peaks in the PBSLM6, which are O-H characteristic peaks of  $3550\text{ cm}^{-1}$ ,  $3410\text{ cm}^{-1}$ ,  $1690\text{ cm}^{-1}$ ,  $1620\text{ cm}^{-1}$  and S-O characteristic peaks of  $1120\text{ cm}^{-1}$ ,  $673\text{ cm}^{-1}$  and  $604\text{ cm}^{-1}$ , respectively. The asymmetric O-H stretching vibration of  $\text{Al(OH)}_6$  octahedron in ettringite is analyzed, and the band at  $3350\text{ cm}^{-1}$  is caused by O-H stretching vibration (Wang et al., 2023). The O-H part of  $3410\text{ cm}^{-1}$ ,  $1690\text{ cm}^{-1}$ ,  $1620\text{ cm}^{-1}$  is related to the bonding water formed by tectonic water. In addition, the signals at  $1120\text{ cm}^{-1}$ ,  $673\text{ cm}^{-1}$  and  $604\text{ cm}^{-1}$  are identified as composite bands composed of  $\delta(\text{Al}-\text{O}-\text{H})$ ,  $\delta(\text{S}-\text{O})$  and  $\delta(\text{Ca}-\text{O}-\text{H})$ , and their strength is significantly affected by gypsum content (Gesoglu et al., 2016).

**3.6.2.3. SEM analysis.** As exhibited in Fig. 26, the hydration products of the PBSLM are mostly plate-like or columnar calcium sulfate dihydrate crystals, with a high degree of self-shape. At the same time, there are some amorphous cementitious materials C-S-H and needle-like AFt structure (Chen et al., 2022). The plate-like or columnar crystals are intertwined to form a dense hydration product hardened body. The reason for the less porosity of PBSLM is mainly due to the hydration calcium silicate gel generated by the hydra-

**Table 21**

Comparison of mechanical properties of PBSLM6 sample with standard values.

NO.	Project	Test value	Standard value (JC/T1023)
1	0 min-fluidity/mm	150	$145 \pm 5$
2	30 min-fluidity/mm	154	$\geq 140$
3	24 h-flexural strength/MPa	5.7	$\geq 2.0$
4	24 h-compressive strength/MPa	10.6	$\geq 5.0$

**Table 22**

XRF test results of PBSLM6/%,mass.

Sample	$\text{SO}_3$	$\text{CaO}$	$\text{SiO}_2$	$\text{MgO}$	$\text{Al}_2\text{O}_3$	$\text{Fe}_2\text{O}_3$	$\text{P}_2\text{O}_5$	$\text{K}_2\text{O}$	Others
PG	45.02	38.48	8.86	2.76	1.66	1.18	1.07	0.35	3.25

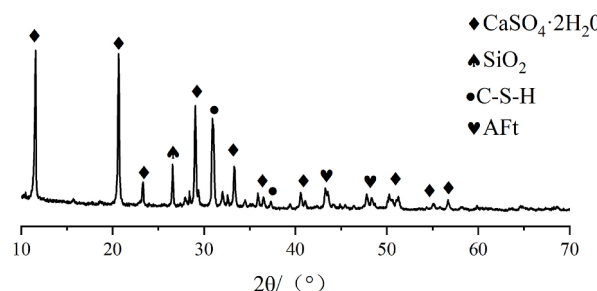


Fig. 24. XRD test results of PBSLM6.

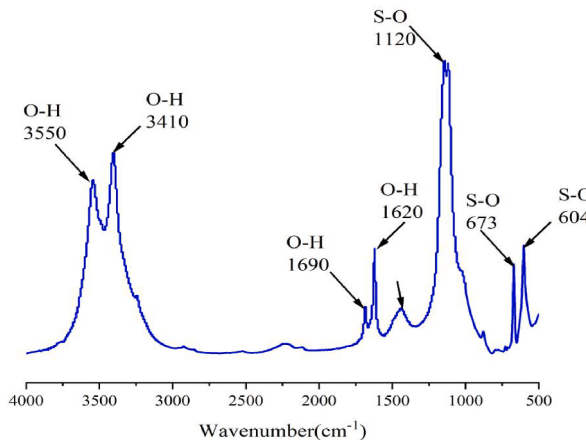


Fig. 25. The FT-IR test of PBSLM6.

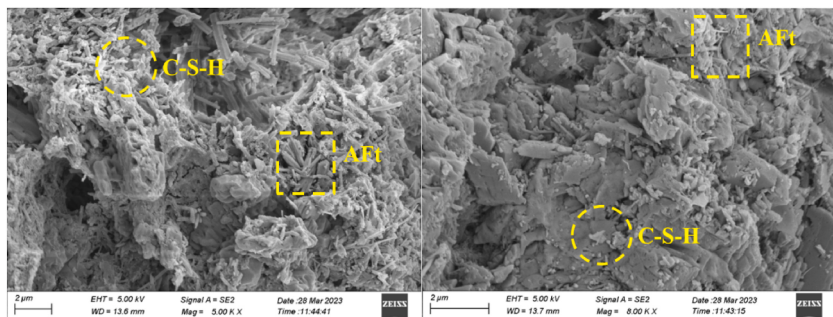
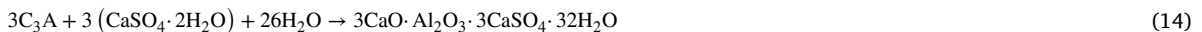


Fig. 26. The SEM of PBSLM6.

tion of ordinary portland cement and the reaction of tricalcium aluminate contained in ordinary portland cement with gypsum to form ettringite ( $\text{C}-\text{S}-\text{H}$ , Aft formation reaction formula, as shown in [formula \(13\)](#) and [\(14\)](#) respectively), which will fill the pores of PBSLM, making PBSLM more dense, thereby improving the strength of gypsum-based self-leveling mortar ([Silva et al., 2023](#)).



**3.6.2.4. EDS analysis** *The*. As shows [Fig. 27](#), the PBSLM6 contains Ca, S, O, Si, and other elements. Compared with the pollutants contained in the powder PG after hydration ([Fig. 15 f](#)), it can be found that the content of F and P decreased significantly, from 0.39 wt % and 0.32 wt % after hydration of MPG to 0.17 wt % and 0.00 wt %; the content of heavy metal Cr decreased from 0.04 wt % to 0 after MPG hydration. However, As and Cd elements increased slightly, from 0 wt % and 0.05 wt % after MPG hydration to 0.54 wt % and 0.1 wt %, which may be caused by heavy metal elements contained in cement. Whether the slight increase of heavy metal elements will affect the environment needs to be further explored.

### 3.6.3. Water immersion analysis of heavy metals in PBSLM6

Because PG is class II solid waste, it contains heavy metals and other pollutants. Relevant studies have indicated that As, Cr, Hg, and Cd elements were mainly present in PG ([Wang et al., 2023](#)). In this paper, a small amount of heavy metal elements were also found by SEM-EDS detection of PBSLM. In order to ensure the safety of heavy metals in the use of PBSLM, the leaching test of the heavy metal aqueous solution was carried out in this paper. The standard value is selected from the Chinese standard “*Integrated Wastewater Discharge Standard*” (GB8978).

It is not difficult to find in [Table 23](#) that the detection results of As Hg and Cd elements are 0.0 mg/L. Although the detection value of the Cr element is 0.1 mg/L, it is far lower than the standard value of  $\leq 1.5$  mg/L. Although PG raw materials contain some heavy metal elements, the content of heavy metal elements decreased significantly after being made into the PBSLM. It was much lower than the standard value. Therefore, we can believe that the heavy metal elements in PBSLM have no safety risks to environmental safety and human health.

### 3.6.4. Economic analysis of PBSLM

China's natural gypsum consumption ranks first in the world, but natural gypsum is a non-renewable resource. By-product gypsum can be reprocessed in many fields to replace natural gypsum completely. Even in today's construction industry, by-product gypsum

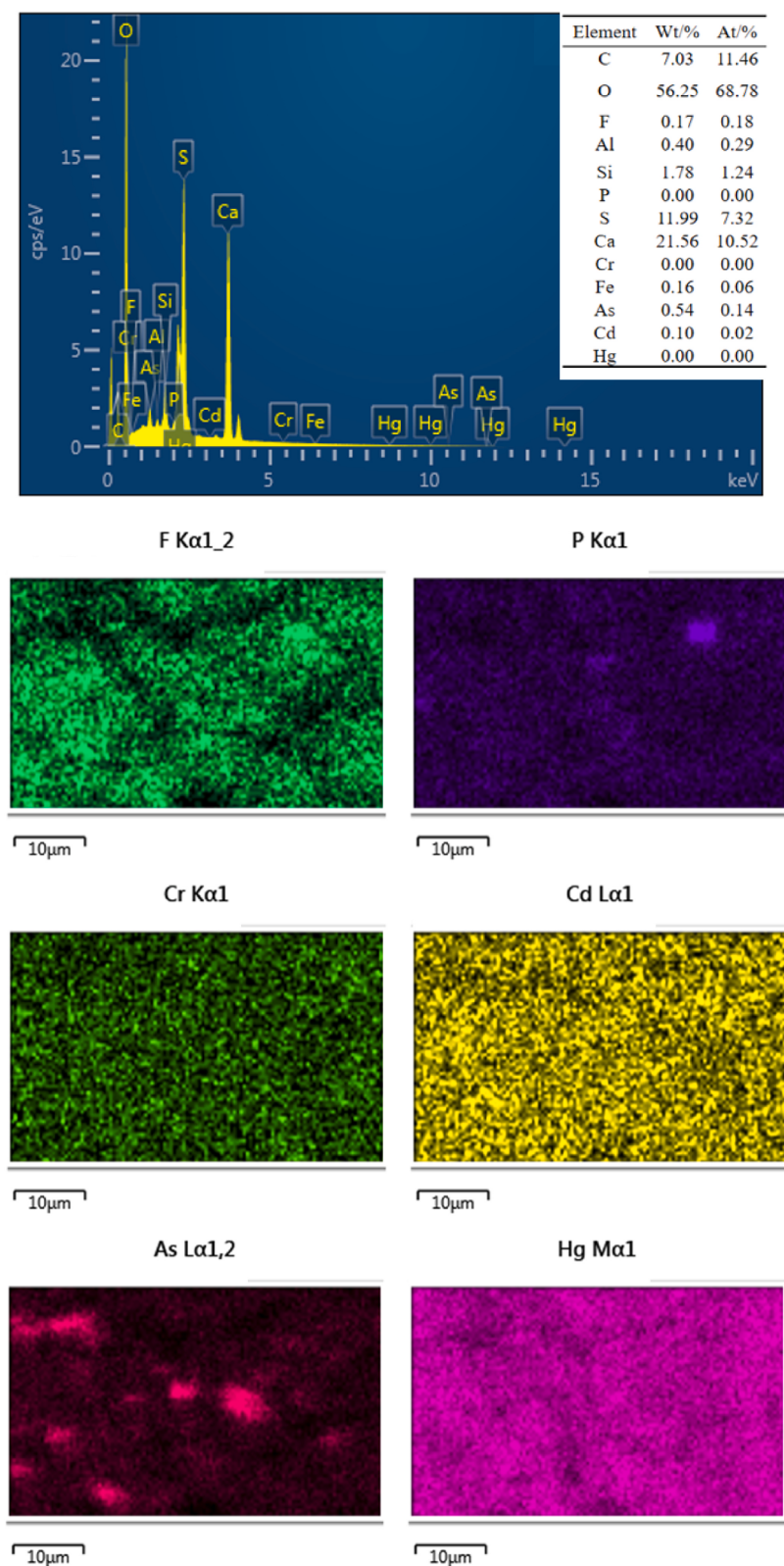


Fig. 27. The EDS of PBSLM6.

**Table 23**

Detection results of heavy metal leaching in aqueous solution of PBSLM6 (mg/L).

NO.	As	Cr	Hg	Cd
Test value	0.0	0.1	0.0	0.0
Standard value	≤0.5	≤1.5	≤0.05	≤0.1

still has certain advantages. Therefore, it is an inevitable trend for the future development of the construction industry to use PG instead of natural gypsum as the raw material of gypsum products in construction projects. In the context of the 'Dual-Carbon' era, there are fewer and fewer production lines for producing high-strength gypsum and building gypsum powder from natural gypsum nationwide. At present, GBSLM is mainly prepared by desulfurized gypsum. If a PBSLM that can replace desulfurized gypsum in terms of performance and economy is developed, the resource utilization rate of PG can be significantly improved. At the same time, it can reduce construction costs and bring considerable economic benefits.

In this paper, the production of 1-ton of PBSLM and desulfurization of gypsum based self-leveling mortar raw material from the production cost of economic analysis and comparison.

Tables 24 and 25 exhibited that the raw material price for producing 1-ton of PBSLM is 311.33 Yuan, according to the current market price. The raw material price for producing one ton of desulfurized gypsum-based self-leveling mortar is 363.85 Yuan. For every ton of PBSLM produced, the production cost can be saved by 52.52 Yuan, and the production cost can be reduced by about 15%. Based on the raw materials cost, the PBSLM developed in this paper is more economical than the desulfurization gypsum-based self-leveling mortar.

### 3.7. Construction of safety utilization evaluation template for general solid waste

Solid waste is a double-edged sword. On the one hand, it poses a certain harm to the ecological environment; on the other hand, with appropriate pretreatment, it can be transformed into raw materials. Therefore, the establishment of a comprehensive and systematic solid waste evaluation system is crucial to reducing pollution and enhancing the recycling rate (Wu et al., 2022). This paper establishes a solid waste heavy metal safety risk assessment model, as depicted in Fig. 28. The model is divided into four main sections: hazard identification, exposure risk, risk characterization, and risk control. The hazard identification section involves data investigation, content analysis of heavy metals in solid waste, and an analysis of potential environmental exposure. Exposure risk establishes different mathematical models for heavy metals in both the natural environment and human health (e.g., single-factor index method, potential ecological risk assessment, the U.S. EPA human health risk assessment model). Risk characterization involves running mathematical models to calculate single and cumulative hazard quotients, comparing them with respective standards to determine the presence of heavy metal safety risks. If the risk assessment value exceeds the standard, the process proceeds to the risk control stage. In this stage, calculations are made to determine the heavy metal risk control values that the raw materials should meet af-

**Table 24**

1-ton PBSLM raw material cost.

NO.	Project	Price/Yuan ¥/t	Consumption proportion/%	Cost ¥/Yuan
1	MPG	200	63.11	126.22
2	Heavy calcium powder	240	14.34	34.42
3	Sand	200	14.34	28.69
4	Cement	400	7.65	30.60
5	Retarding admixture	5300	0.06	3.04
6	Water reducing admixture	15,000	0.31	45.90
7	Cellulose ether	52,000	0.06	29.83
8	Defoaming admixture	10,000	0.10	9.56
9	Air-entraining agent	8000	0.04	3.06
Total			100	311.33

**Table 25**

1-ton desulfurization gypsum based self-leveling mortar raw material cost.

NO.	Project	Price/Yuan ¥/t	Consumption proportion/%	Cost ¥/Yuan
1	Desulfurized gypsum powder	300	56.81	170.42
2	Heavy calcium powder	240	30.30	72.71
3	Sand	200	4.73	9.47
4	Cement	400	7.57	30.28
5	Retarding admixture	5300	0.23	12.04
6	Water reducing admixture	15,000	0.19	28.40
7	Cellulose ether	52,000	0.06	29.54
8	Defoaming admixture	10,000	0.09	9.47
9	Air-entraining agent	8000	0.02	1.51
Total				363.85

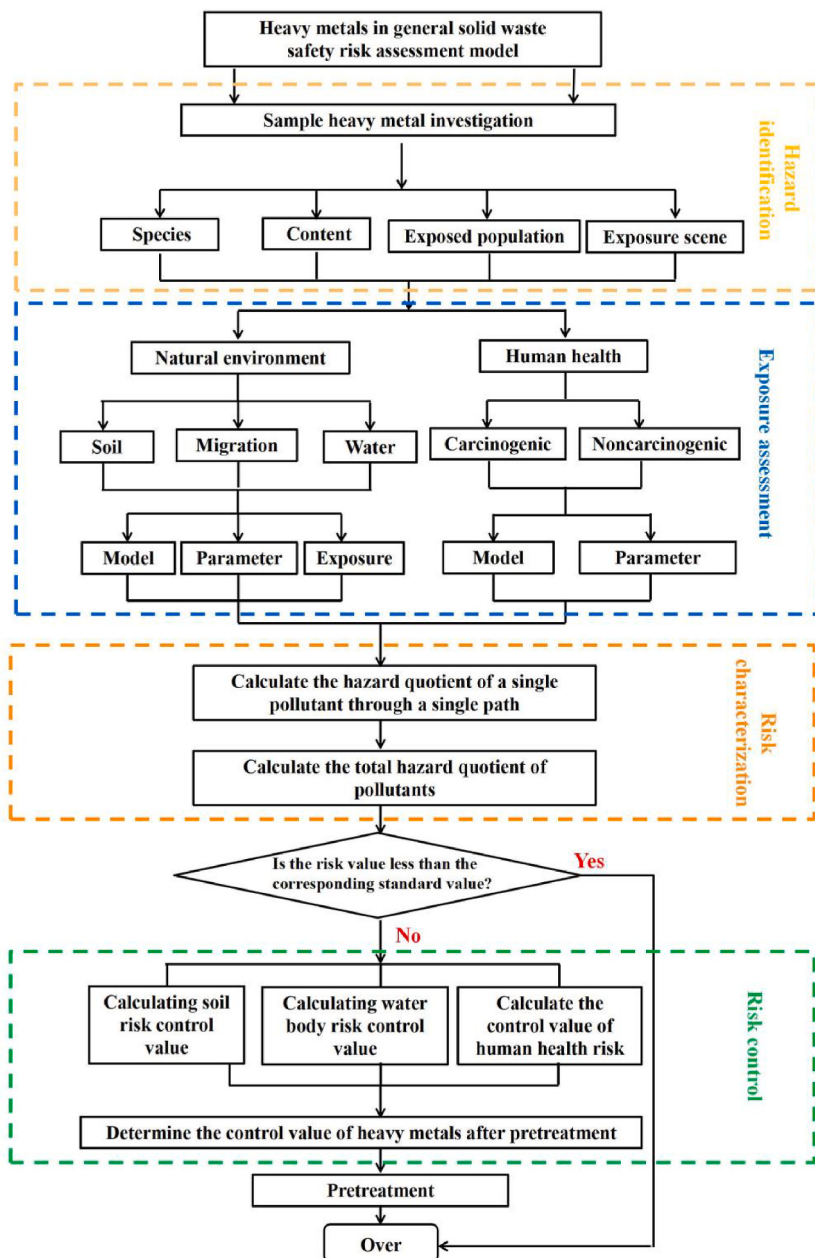


Fig. 28. Heavy metals in general solid waste safety risk assessment model.

ter processing. The establishment of this model addresses current shortcomings in China's solid waste heavy metal safety control, ensuring that the safe utilization of heavy metals in the recycling of solid waste resources is referenced.

#### 4. Conclusion

The MPG macro performance, microstructure, thermodynamic modification mechanism, modification process of migration and transformation of heavy metals and ecological security assessment analysis concluded were as follows.

- (1) Ball milling could effectively modify the particle size distribution, leading to an elevated content of hemihydrate calcium sulfate and anhydrous calcium sulfate with increasing temperature. Following pre-treatments at 180 °C/10 h and 195 °C/7 h/10 h, the mechanical properties of PG satisfied the standard requirements of "Building Gypsum" (GB/T9776). Notably, the mechanical properties were optimal at 195 °C/10 h, demonstrating bending and compressive strengths of 3.33 MPa and 4.77 MPa, respectively.

- (2) During the transformation from PG to MPG, the formation of substitutional solid solutions between heavy metals Cd<sup>2+</sup>, Hg<sup>2+</sup>, Cr<sup>3+</sup> and Ca<sup>2+</sup>, Fe<sup>3+</sup> in PG, along coupled with the larger specific surface area of hemihydrate calcium sulfate and the grinding effect, can, to some extent, reduce the content of heavy metals. During the conversion process from PG to MPG, heavy metals Cd<sup>2+</sup>, Hg<sup>2+</sup>, Cr<sup>3+</sup> formed substitutional solid solutions with Ca<sup>2+</sup>, Fe<sup>3+</sup>. Additionally, the relatively large specific surface area of calcium sulfate hemihydrate and the grinding action contributed to some extent to the reduction of heavy metal content. This reduction was the main reason for their decreased levels. In the process from MPG to HPG, the adsorption of colloidal dicalcium sulfate was the primary reason for a further decrease in the content of certain heavy metals. However, it was worth noting that the increase in As content is mainly attributed to the chemical reaction between H<sub>2</sub>AsO<sub>4</sub><sup>-</sup> and Ca<sup>2+</sup>, resulting in the formation of Ca(H<sub>2</sub>AsO<sub>4</sub>)<sub>2</sub>. Ca(H<sub>2</sub>AsO<sub>4</sub>)<sub>2</sub> was insoluble in water but soluble in acid, leading to an increase in the measured heavy metal content during ICP testing. The growth of the Cd element was primarily due to the dissolution of iron oxides present in MPG during the initial stages of hydration.
- (3) There was no environmental safety risk associated with heavy metals in MPG. However, non-carcinogenic risks from oral ingestion exist for As and Cr. Risk control values for the application of PG in different scenarios were obtained through the analysis model of heavy metal safety assessment for solid waste. Road control value: As < 0.35 mg/kg, Cd < 0.12 mg/kg. Agriculture control values: As < 0.3 mg/kg, Cd < 0.10 mg/kg. Building materials control values: As < 0.25 mg/kg, Cd < 0.08 mg/kg.
- (4) The PBSLM prepared with an MPG dosage of 300 g and cement dosage of 40 g exhibits the best mechanical properties. Its 24-h bending and compressive strengths were 5.7 MPa and 10.6 MPa, respectively, meeting the standards for "Gypsum-Based Self-Leveling Mortar." Additionally, the leaching values of heavy metals in PBSLM were significantly lower than the limits set by the Chinese standard for "Comprehensive Discharge Standards for Sewage". In terms of cost-effectiveness compared to desulfurized gypsum-based self-leveling mortar, it was found that PBSLM has a clear economic advantage, saving up to 15% of costs.

#### CRediT authorship contribution statement

**Chao-qiang Wang:** Conceptualization, Data curation, Formal analysis, Funding acquisition, Investigation, Methodology, Project administration, Resources, Supervision, Writing – review & editing. **Ze-yuan Wang:** Investigation, Methodology, Writing – original draft, Writing – review & editing. **Jing-wen Wang:** Investigation, Methodology. **Huan Zhang:** Methodology, Project administration, Resources. **De-ming Huang:** Investigation, Methodology, Project administration.

#### Declaration of competing interest

The authors declare that they have no known competing financial interests or personal relationships that could have appeared to influence the work reported in this paper.

#### Data availability

Data will be made available on request.

#### Acknowledgements

This work was financially supported by Science and technology research project of Chongqing Municipal Education Commission of China (KJQN202100723), Chongqing technology innovation and application development special key project(CSTB2022TIAD-KPX0111), Open Project of State Key Laboratory of Solid Waste Reuse for Building Materials(SWR-2023-003), Project Supported by Chongqing Municipal Construction Science and Technology Plan (Chengkezi 2022 No. 2-8).

#### References

- Al-Hwaiti, M., Ibrahim, K.A., Harrara, M., 2019. Removal of heavy metals from waste phosphogypsum materials using polyethylene glycol and polyvinyl alcohol polymers. *Arab. J. Chem.* 12 (8), 3141–3150.
- Beldjilali, S., Bougara, A., Aguiar, J., Bouhamou, N.-E., Dabbebi, R., 2020. Properties of a new material based on a gypsum matrix incorporating waste brick. *Construct. Build. Mater.* 259, 120416.
- Bumanis, G., Zorica, J., Bajare, D., Korjakins, A., 2018. Technological properties of phosphogypsum binder obtained from fertilizer production waste. *Energy Proc.* 147, 301–308.
- Chen, S., Chen, J., He, X., Su, Y., Jin, Z., Wang, B., 2022. Micromicelle-mechanical coupling method for high-efficiency phosphorus removal and whiteness improvement of phosphogypsum. *Construct. Build. Mater.* 354, 129220.
- Cao, W., Yi, W., Li, J., Peng, J., Yin, S., 2021. A facile approach for large-scale recovery of phosphogypsum: an insight from its performance. *Construct. Build. Mater.* 309, 125190.
- Cao, W., Yi, W., Peng, J., Li, J., Yin, S., 2022. Recycling of phosphogypsum to prepare gypsum plaster: effect of calcination temperature. *J. Build. Eng.* 45, 103511.
- Chai, L., Wang, Y., Wang, X., Ma, L., Cheng, Z., Su, L., 2021. Pollution characteristics, spatial distributions, and source apportionment of heavy metals in cultivated soil in Lanzhou, China. *Ecol. Indicat.* 125, 107507.
- Chen, C., Ma, F., He, T., Kang, Z., Wang, Y., Shi, C., 2022. Improved water and efflorescence resistance of flue gas desulfurization gypsum-based composites by generating hydrophobic coatings. *J. Clean. Prod.* 371, 133711.
- Chen, X., Liu, Y., Wu, Q., Ding, Y., Wang, Q., Tang, W., Zhu, B., 2022a. Study on physical and chemical characteristics of  $\beta$ -hemihydrate phosphogypsum. *Case Stud. Constr. Mater.* 17, e01461.
- Chen, X., Wang, Q., Ding, Y., Wu, Q., Chen, Y., Liu, Y., 2022b. Influence mechanism of alkaline environment on the hydration of hemihydrate phosphogypsum: a comparative study of various alkali. *Construct. Build. Mater.* 353, 129070.
- Costa, R.P., de Medeiros, M.H.G., Rodriguez Martinez, E.D., Quarcioni, V.A., Suzuki, S., Kirchheim, A.P., 2022. Effect of soluble phosphate, fluoride, and pH in Brazilian

- phosphogypsum used as setting retarder on Portland cement hydration. *Case Stud. Constr. Mater.* 17, e01413.
- Değirmenci, N., 2008. Utilization of phosphogypsum as raw and calcined material in manufacturing of building products. *Construct. Build. Mater.* 22 (8), 1857–1862.
- Ding, C., Sun, T., Shui, Z., Xie, Y., Ye, Z., 2022. Physical properties, strength, and impurities stability of phosphogypsum-based cold-bonded aggregates. *Construct. Build. Mater.* 331, 127307.
- Dogan, G.M., Arbag, H., Koyuncu, D.D.E., 2022. Effect of graphene-based additives on mechanical strength and microstructure of gypsum plaster. *Mater. Today Commun.* 33, 104555.
- Dong, B., Zhang, R., Gan, Y., Cai, L., Freidenreich, A., Wang, K., Guo, T., Wang, H., 2019. Multiple methods for the identification of heavy metal sources in cropland soils from a resource-based region. *Sci. Total Environ.* 651, 3127–3138.
- Fatoki, J.O., Badmus, J.A., 2022. Arsenic as an environmental and human health antagonist: a review of its toxicity and disease initiation. *J. Hazardous Mater. Adv.* 5, 100052.
- Follner, S., Wolter, A., Preusser, A., Indris, S., Silber, C., Follner, H., 2002. The setting behaviour of  $\alpha$ -and  $\beta$ -CaSO<sub>4</sub>·0.5 H<sub>2</sub>O as a function of crystal structure and morphology. *Cryst. Res. Technol.* 37, 1075–1087.
- Geraldo, R.H., Costa, A.R.D., Kanai, J., Silva, J.S., Souza, J.D., Andrade, H.M.C., Gonçalves, J.P., Fontanini, P.S.P., Camarini, G., 2020. Calcination parameters on phosphogypsum waste recycling. *Construct. Build. Mater.* 256, 119406.
- Gesoglu, M., Güneyisi, E., Nahhab, A.H., Yazıcı, H., 2016. The effect of aggregates with high gypsum content on the performance of ultra-high strength concretes and Portland cement mortars. *Construct. Build. Mater.* 110, 346–354.
- Gijbels, K., Nguyen, H., Kinnunen, P., Samyn, P., Schroyers, W., Pontikes, Y., Schreurs, S., Ilikainen, M., 2020a. Radiological and leaching assessment of an ettringite-based mortar from ladle slag and phosphogypsum. *Cement Concr. Res.* 128, 105954.
- He, H., Yang, B., Wu, D., Gao, X., Fei, X., 2022. Applications of crushing and grinding-based treatments for typical metal-containing solid wastes: detoxification and resource recovery potentials. *Environ. Pollut.* 120034.
- Huang, T., Yuan, Q., Zuo, S., Xie, Y., Shi, C., 2022. New insights into the effect of gypsum on hydration and elasticity development of C3S paste during setting. *Cement Concr. Res.* 159, 106860.
- Jalali, J., Gaudin, P., Ammar, E., Lebeau, T., 2020. Bioaugmentation coupled with phytoextraction for the treatment of Cd and Sr, and reuse opportunities for phosphogypsum rare earth elements. *J. Hazard Mater.* 399, 122821.
- Jia, J., Bai, J., Xiao, R., Tian, S., Wang, D., Wang, W., Zhang, G., Cui, H., Zhao, Q., 2022. Fractionation, source, and ecological risk assessment of heavy metals in cropland soils across a 100-year reclamation chronosequence in an estuary, South China. *Sci. Total Environ.* 807, 151725.
- Kalkan, S.O., Yavaş, A., Güler, S., Torman Kayalar, M., Sütçü, M., Gündüz, L., 2022. An experimental approach to a cementitious lightweight composite mortar using synthetic wollastonite. *Construct. Build. Mater.* 341, 127911.
- Kashem, M.A., Singh, B.R., 2001. Metal availability in contaminated soils: I. Effects of flooding and organic matter on changes in Eh, pH and solubility of Cd, Ni and Zn. *Nutrient Cycl. Agroecosyst.* 61 (3), 247–255.
- Komarineni, S., Breval, E., Roy, D.M., Roy, R., 1988. Reactions of some calcium silicates with metal cations. *Cement Concr. Res.* 18 (2), 204–220.
- Li, B., Li, L., Chen, X., Ma, Y., Zhou, M., 2022. Modification of phosphogypsum using circulating fluidized bed fly ash and carbide slag for use as cement retarder. *Construct. Build. Mater.* 338, 127630.
- Li, H., Ji, H., 2017. Chemical speciation, vertical profile and human health risk assessment of heavy metals in soils from coal-mine brownfield, Beijing, China. *J. Geochem. Explor.* 183, 22–32.
- Li, H., Xu, C., Li, L., Chen, Q., Yang, X., Wang, W., Liu, R., 2020. Insight into the influences of  $\beta$ -hemihydrate and dihydrate gypsum on the properties and phase conversion of white calcium aluminate cement. *Construct. Build. Mater.* 263, 120106.
- Li, J., Chang, J., Wang, T., Zeng, T., Li, J., Zhang, J., 2022. Effects of phosphogypsum on hydration properties and strength of calcium aluminate cement. *Construct. Build. Mater.* 347, 128398.
- Li, X., Zhang, Q., 2021. Dehydration behaviour and impurity change of phosphogypsum during calcination. *Construct. Build. Mater.* 311, 125328.
- Li, Y., Luo, W., Li, G., Wang, K., Gong, X., 2018. Performance of phosphogypsum and calcium magnesium phosphate fertilizer for nitrogen conservation in pig manure composting. *Bioresour. Technol.* 250, 53–59.
- Li, Z., Wang, X., Hou, Y., Wu, Z., 2022. Optimization of mechanical properties and water absorption behavior of building gypsum by ternary matrix mixture. *Construct. Build. Mater.* 350, 128910.
- Liu, S., Ouyang, J., Ren, J., 2020. Mechanism of calcination modification of phosphogypsum and its effect on the hydration properties of phosphogypsum-based supersulfated cement. *Construct. Build. Mater.* 243, 118226.
- Liu, S., Sun, Q., Asselin, E., Li, Z., 2022. Crystallization kinetics of large-sized columnar  $\alpha$ -hemihydrate gypsum by reaction of waste CaCl<sub>2</sub> and Al<sub>2</sub>(SO<sub>4</sub>)<sub>3</sub> without crystal modifiers. *J. Cryst. Growth* 596, 126817.
- Liu, X., Zhai, Y., Zhu, Y., Liu, Y., Chen, H., Li, P., Peng, C., Xu, B., Li, C., Zeng, G., 2015. Mass concentration and health risk assessment of heavy metals in size-segregated airborne particulate matter in Changsha. *Sci. Total Environ.* 517, 215–221.
- Lopes, G., Guilherme, L.R.G., Costa, E.T.S., Curi, N., Penha, H.G.V., 2013. Increasing arsenic sorption on red mud by phosphogypsum addition. *J. Hazard Mater.* 262, 1196–1203.
- Lü, Q., Xiao, Q., Wang, Y., Wen, H., Han, B., Zheng, X., Lin, R., 2021. Risk assessment and hotspots identification of heavy metals in rice: a case study in Longyan of Fujian province, China. *Chemosphere* 270, 128626.
- Mallongi, A., Astuti, R.D.P., Amiruddin, R., Hatta, M., Rauf, A.U., 2022. Identification source and human health risk assessment of potentially toxic metal in soil samples around karst watershed of Pangkajene, Indonesia. *Environ. Nanotechnol. Monit. Manag.* 17, 100634.
- Mashifana, T.P., 2019. Chemical treatment of phosphogypsum and its potential application for building and construction. *Procedia Manuf.* 35, 641–648.
- Meskini, S., Mechoua, I., Benmansour, M., Remmal, T., Samdi, A., 2023. Environmental investigation on the use of a phosphogypsum-based road material: radiological and leaching assessment. *J. Environ. Manag.* 345, 118597.
- Massaro, F.R., Rubbo, M., Aquilano, D., 2010. Theoretical equilibrium morphology of gypsum (CaSO<sub>4</sub>·2H<sub>2</sub>O). 1. A syncretic strategy to calculate the morphology of crystals. *Cryst. Growth Des.* 10 (7), 2870–2878.
- Mi, Y., Chen, D., Wang, S., 2018. Utilization of phosphogypsum for the preparation of  $\alpha$ -calcium sulfate hemihydrate in chloride-free solution under atmospheric pressure. *J. Chem. Technol. Biotechnol.* 93 (8), 2371–2379.
- Miroslav, H., Pavel, H., Josef, B., Jarmila, K., 2021. Arsenic as a contaminant of struvite when recovering phosphorus from phosphogypsum wastewater. *J. Taiwan Inst. Chem. Eng.* 129, 91–96.
- Mittal, A., Rakshit, D., 2020. Utilization of cement rotary kiln waste heat for calcination of phosphogypsum. *Therm. Sci. Eng. Prog.* 20, 100729.
- Nomura, Y., Fujiwara, K., Takada, M., Nakai, S., Hosomi, M., 2008. Lead immobilization in mechanochemical fly ash recycling. *J. Mater. Cycles Waste Manag.* 10 (1), 14–18.
- Okoye, E.A., Ezejiofor, A.N., Nwaogazie, I.L., Fazzoli, C., Orisakwe, O.E., 2022. Heavy metals and arsenic in soil and vegetation of Niger Delta, Nigeria: ecological risk assessment. *Case Stud. Chem. Environ. Eng.* 6, 100222.
- Oliveira, T.V., Cordeiro, L.d.N.P., Bessa, S.A.L., 2022. Experimental study of self-leveling mortars produced with recycled concrete aggregates. *Case Stud. Constr. Mater.* 17, e01294.
- Peng, X., Zheng, J., Liu, Q., Hu, Q., Sun, X., Li, J., Liu, W., Lin, Z., 2021. Efficient removal of iron from red gypsum via synergistic regulation of gypsum phase transformation and iron speciation. *Sci. Total Environ.* 791, 148319.
- Rosales, J., Pérez, S.M., Cabrera, M., Gázquez, M.J., Bolívar, J.P., de Brito, J., Agrela, F., 2020. Treated phosphogypsum as an alternative set regulator and mineral addition in cement production. *J. Clean. Prod.* 244, 118752.
- Sagitha, A., Puspita, A.D., Dwi, R.P., Salasa, A., 2021. Optimization of gypsum composition against setting time and compressive strength in clinker for PCC (Portland Composite Cement). *IOP Conference Series: Materials Science and Engineering.* IOP Publishing, 012116.
- Saddam Alwan, A., Al-Shammari, A.J., Hadi Jumaa, N., Mohamad Ali, I., Habeeb Hussain, T., Samir Naje, A., 2022. Experimental investigation on the effect of incorporating nanomaterials on some properties of self-compacting cementitious mortar. *Mater. Today: Proc.* 60, 1570–1574.

- Silva, D.B.P., Lima, N.B., Lima, V.M.E., Estolano, A.M.L., Nascimento, H.C.B., Vilemen, P., Padron-Hernández, E., Carneiro, A.M.P., Lima, N.B.D., Povoas, Y.V., 2023. Producing a gypsum-based self-leveling mortar for subfloor modified by polycarboxylate admixture (PCE). *Construct. Build. Mater.* 364, 130007.
- Singh, M., Garg, M., 2000. Making of anhydrite cement from waste gypsum. *Cement Concr. Res.* 30 (4), 571–577.
- Singh, N.B., Middendorf, B., 2007. Calcium sulphate hemihydrate hydration leading to gypsum crystallization. *Prog. Cryst. Growth Char. Mater.* 53 (1), 57–77.
- Stephan, D., Mallmann, R., Knöfel, D., Härdtl, R., 1999. High intakes of Cr, Ni, and Zn in clinker: Part I. Influence on burning process and formation of phases. *Cement Concr. Res.* 29 (12), 1949–1957.
- Sun, C.J., Li, M.-G., Gau, S.-H., Wang, Y.-H., Jan, Y.-L., 2011. Improving the mechanical characteristics and restraining heavy metal evaporation from sintered municipal solid waste incinerator fly ash by wet milling. *J. Hazard Mater.* 195, 281–290.
- Tanabe, K., Takeshita, T., 1967. Catalytic activity and acidic property of solid metal sulfates. *Adv. Catal.* 17, 315–349.
- Taplin, J.H., 2004. Hydration kinetics of calcium sulphate hemihydrate—a comment. *Cement Concr. Res.* 34 (10), 1963.
- Wang, C.Q., Wang, Z.Y., Huang, D.M., Huang, Q.C., Chen, Y., Zhang, H., Shui, Z.-H., 2023. Recovery and recycling core of phosphogypsum: characteristic hazardous elements risk assessment and analysis. *Process Saf. Environ. Protect.* 170, 738–756.
- Wang, J., 2020. RETRACTED: utilization effects and environmental risks of phosphogypsum in agriculture: a review. *J. Clean. Prod.* 276, 123337.
- Wang, Q., Jia, R., 2019. A novel gypsum-based self-leveling mortar produced by phosphorus building gypsum. *Construct. Build. Mater.* 226, 11–20.
- Wang, S., Kalkhajeh, Y.K., Qin, Z., Jiao, W., 2020. Spatial distribution and assessment of the human health risks of heavy metals in a retired petrochemical industrial area, south China. *Environ. Res.* 188, 109661.
- Wang, X., Guo, M.-Z., Yue, G., Li, Q., Ling, T.-C., 2022. Synthesis of high belite sulfoaluminate cement with high volume of mixed solid wastes. *Cement Concr. Res.* 158, 106845.
- Wang, Z., Luo, P., Zha, X., Xu, C., Kang, S., Zhou, M., Nover, D., Wang, Y., 2022. Overview assessment of risk evaluation and treatment technologies for heavy metal pollution of water and soil. *J. Clean. Prod.* 134043.
- Wang, Z., Shui, Z., Sun, T., Hu, T., Xiao, X., Fan, J., 2023. Reutilization of gangue wastes in phosphogypsum-based excess-sulphate cementitious materials: effects of wet co-milling on the rheology, hydration and strength development. *Construct. Build. Mater.* 363, 129778.
- Wei, Z., Deng, Z., 2022. Research hotspots and trends of comprehensive utilization of phosphogypsum: bibliometric analysis. *J. Environ. Radioact.* 242, 106778.
- Wu, C.-W., Sun, C.-J., Gau, S.-H., Hong, C.-L., Chen, C.-G., 2013. Mechanochemically induced synthesis of anorthite in MSWI fly ash with kaolin. *J. Hazard Mater.* 244–245, 412–420.
- Wu, F., Chen, B., Qu, G., Liu, S., Zhao, C., Ren, Y., Liu, X., 2022a. Harmless treatment technology of phosphogypsum: directional stabilization of toxic and harmful substances. *J. Environ. Manag.* 311, 114827.
- Wu, F., Ren, Y., Qu, G., Liu, S., Chen, B., Liu, X., Zhao, C., Li, J., 2022b. Utilization path of bulk industrial solid waste: a review on the multi-directional resource utilization path of phosphogypsum. *J. Environ. Manag.* 313, 114957.
- Wu, G., Wang, L., Yang, R., Hou, W., Zhang, S., Guo, X., Zhao, W., 2022. Pollution characteristics and risk assessment of heavy metals in the soil of a construction waste landfill site. *Ecol. Inf.* 70, 101700.
- Xiang, J., Qiu, J., Zheng, P., Sun, X., Zhao, Y., Gu, X., 2023. Usage of biowashing to remove impurities and heavy metals in raw phosphogypsum and calcined phosphogypsum for cement paste preparation. *Chem. Eng. J.* 451, 138594.
- Xie, L., Zhou, Y., Xiao, S., Miao, X., Murzataev, A., Kong, D., Wang, L., 2022. Research on basalt fiber reinforced phosphogypsum-based composites based on single factor test and RSM test. *Construct. Build. Mater.* 316, 126084.
- Xu, T., Wang, L.a., Wang, X., Li, T., Zhan, X., 2018. Heavy metal pollution of oil-based drill cuttings at a shale gas drilling field in Chongqing, China: a human health risk assessment for the workers. *Ecotoxicol. Environ. Saf.* 165, 160–163.
- Yang, J., Liu, W., Zhang, L., Xiao, B., 2009. Preparation of load-bearing building materials from autoclaved phosphogypsum. *Construct. Build. Mater.* 23 (2), 687–693.
- Yang, J., Sun, Y., Wang, Z., Gong, J., Gao, J., Tang, S., Ma, S., Duan, Z., 2022. Heavy metal pollution in agricultural soils of a typical volcanic area: risk assessment and source apportionment. *Chemosphere* 304, 135340.
- Yang, L., Zhang, Y., Yan, Y., 2016. Utilization of original phosphogypsum as raw material for the preparation of self-leveling mortar. *J. Clean. Prod.* 127, 204–213.
- Yelatontsev, D., Mukhachev, A., 2021. Utilizing of sunflower ash in the wet conversion of phosphogypsum – a comparative study. *Environ. Challenges* 5, 100241.
- Zarei, M.M., Hosseini, M., Mohammadi, A.H., Moosavi, A., 2021. Model development for estimating calcium sulfate dihydrate, hemihydrate, and anhydrite solubilities in multicomponent acid and salt containing aqueous solutions over wide temperature ranges. *J. Mol. Liq.* 328, 115473.
- Zhang, S., Xu, X., Memon, S.A., Dong, Z., Li, D., Cui, H., 2018. Effect of calcium sulfate type and dosage on properties of calcium aluminate cement-based self-leveling mortar. *Construct. Build. Mater.* 167, 253–262.
- Zhang, Y., Yang, J., Cao, X., 2020. Effects of several retarders on setting time and strength of building gypsum. *Construct. Build. Mater.* 240, 117927.
- Zhang, Y., Yang, J., Liu, Y., Liu, B., Zhao, F., 2021. Preparation of self-leveling mortar based on anhydrite-II phosphogypsum. *J. Phys. Conf.* 2076 (1), 012035.
- Zheng, T., Qian, C., Su, Y., 2021. Influences of different calcium sources on the early age cracks of self-healing cementitious mortar. *Biochem. Eng. J.* 166, 107849.
- Zhi, Z., Huang, J., Guo, Y., Lu, S., Ma, B., 2017. Effect of chemical admixtures on setting time, fluidity and mechanical properties of phosphorus gypsum based self-leveling mortar. *KSCE J. Civ. Eng.* 21, 1836–1843.
- Zhou, Y., Rao, Y., Zhang, L., Ju, S., Wang, H., 2022. Machine-learning prediction of Vegard's law factor and volume size factor for binary substitutional metallic solid solutions. *Acta Mater.* 237, 118166.
- Zhou, Z., Lu, Y., Zhan, W., Guo, L., Du, Y., Zhang, T.C., Du, D., 2022. Four stage precipitation for efficient recovery of N, P, and F elements from leachate of waste phosphogypsum. *Miner. Eng.* 178, 107420.